ANKARA YILDIRIM BEYAZIT UNIVERSITY

GRADUATE SCHOOL OF NATURAL AND APPLIED SCIENCES



NUMERICAL INVESTIGATION OF INCLINED FLUIDIC OSCILLATOR IN MICROCHANNEL HEAT EXCHANGER

M.Sc. Thesis by

Furkan YEŞİL

Department of Aeronautics and Space Sciences

June, 2023

ANKARA

NUMERICAL INVESTIGATION OF INCLINED FLUIDIC OSCILLATOR IN MICROCHANNEL HEAT TRANSFER

A Thesis Submitted to

The Graduate School of Natural and Applied Sciences of

Ankara Yıldırım Beyazıt University

In Partial Fulfillment of the Requirements for the Degree of Master of Science in Aeronautics and Space Sciences, Department of Aeronautics and Space Sciences

by

Furkan YEŞİL

June, 2023

ANKARA

M.Sc. THESIS EXAMINATION RESULT FORM

We have read the thesis entitled **"NUMERICAL INVESTIGATION OF INCLINED FLUIDIC OSCILLATOR IN MICROCHANNEL HEAT TRANSFER"** completed by **FURKAN YEŞİL** under the supervision of **PROF. DR. VELİ ÇELİK** and we certify that in our opinion it is fully adequate, in scope and in quality, as a thesis for the degree of Master of Science.

Prof. Dr. Veli ÇELİK

Supervisor

Prof. Dr. Adnan SÖZEN

Jury Member

Asst. Prof. Orhan ÖZÇELİK

Jury Member

Prof. Dr. Sadettin ORHAN

Director

Graduate School of Natural and Applied Sciences

ETHICAL DECLARATION

I hereby declare that, in this thesis which has been prepared in accordance with the Thesis Writing Manual of Graduate School of Natural and Applied Sciences,

- All data, information, and documents are obtained in the framework of academic and ethical rules,
- All information, documents, and assessments are presented in accordance with scientific ethics and morals,
- All the materials that have been utilized are fully cited and referenced,
- No change has been made on the utilized materials,
- All the works presented are original,

and in any contrary case of above statements, I accept to renounce all my legal rights.

Date: 14/06/2023 **Signature:**

Name & Surname: Furkan YEŞİL

ACKNOWLEDGMENTS

I would first like to thank Ankara Yıldırım Beyazıt University and TUSAŞ for providing me all technical opportunities. I would like to thank my thesis advisor, Prof. Dr. Veli ÇELİK who always guided me in this research. Whenever I had a question about my thesis or unable to work out a solution, his door was always open to me. Besides, I would also like to thank my family for supporting me at every stage of my life.

2023, 14 June **Furkan YEŞİL**

NUMERICAL INVESTIGATION OF INCLINED FLUIDIC OSCILLATOR IN MICROCHANNEL HEAT EXCHANGER

ABSTRACT

The primary aim of this research was to investigate the enhancement of momentum and thermal energy transfer in a microchannel heat exchanger through the use of fluidic oscillators. To this end, a sweeping jet impingement heat transfer performance was evaluated with varying impact angles, distances between fluidic oscillators, and Re numbers.

This study employed two fluidic oscillators to investigate heat transfer in a microchannel heat exchanger. To enhance the effectiveness of heat transmission in jet cooling, the fluid was oscillated. This allowed it to be calculated how much the flow rate and, consequently, the local Nu value increased, increasing the heat transfer performance. The study was based on the work of Wu Y. et al. validation studies were carried out on the study from the base study and model is validated for 3 Re numbers. Following the validation research, angles of 30, 45, and 60 degrees were evaluated between the fluid oscillator and the channel. Additionally, the distance between the two oscillators was investigated at distances of 7D, 7.5D, and 8D from the center of the outlet hole. A steady heat flux was applied to the channel surface, which served as the impact surface in the model. The fluid's Reynolds range was identified as 3000 to 10000.

The study's findings revealed that increasing the oscillation of the jet flow process improves heat transfer efficiency. Additionally, it was found that when the impact angle grew, the pressure drop and Nu number likewise increased, with a 12 percent improvement in heat transfer being the largest. The heat transmission is found to be positively impacted by shortening the space between the strings, with a maximum improvement of 5.7 percent.

Keywords: Computational Fluid Dynamics, Fluidic Oscillator, Impinging Jet, Heat Transfer Enhancement

MİKROKANALLI ISI DEĞİŞTİRİCİSİNDE EĞİMLİ AKIŞKAN OSİLATÖRÜN SAYISAL İNCELENMESİ

ÖZ

Bu çalışmanın amacı, akışkan osilatörlerin kullanımı yoluyla bir miktro kanallı ısı değiştiricisiside momentum ve ısı transferinin iyileştirmesini araştırmaktır. Bu amaçla, değişken çarpma açıları, akışkan osilatörler arasındaki mesafeler ve Re sayıları ile osile eden çarptırmalı jet akışının ısı transferi performansı değerlendirilmiştir.

Bir mikrokanal ısı eşanjöründe ısı transferini araştırmak için iki akışkan osilatör kullanmıştır. Akışkan, jet soğutmada ısı transferi performansını arttırmak için salınım hareketine maruz bırakıldı. Bu sayede akış hızında ve dolayısıyla yerel Nu değerinde bir artışa neden olarak ısı transferi performansının ne kadar arttırdığı belirlenmiştir. Çalışmada, Wu Y. Ve ark. gerçekleştirdiği çalışma temel alınmıştır.. Temel alınan çalışma 3 farklı Re değerinde gerçekleştirlmiştir ve model doğrulanmıştır. Doğrılama çalışmasından sonra, akışkan osilatör ile kanal arasındaki açı 30°, 45° ve 60° olacak şekilde incelenmiştir. Ayrıca, iki osilatör arasındaki mesafe, çıkış deliği merkezleri arasındaki 7D, 7.5D ve 8D mesafelerde incelenmiştir. Çarpma yüzeyi olarak modellenen kanal yüzeyi, sabit ısı akısına maruz bırakıldı. Akışkanın Reynolds aralığı 3000 ila 10000 olarak belirlendi.

Çalışma sonucunda jet akış işleminin salınımlı hale getirilmesinin ısı transfer performansının artmasına neden olduğu gözlenmiştir. Ayrıca, çarpma açısındaki bir artışın hem basınç düşüşünü hem de Nu sayısını arttırdığı ve ısı trasferindeki en yüksek iyileşmenin yüzde 12.5 olduğu görülmüştür. Son olarak diziler arası mesafenin azaltılmasının ısı transferini olumlu yönde etkileyerek maksimum yüzde 5.7 oranında iyileşme sağladığı belirlenmiştir.

Anahtar Kelimeler: Hesaplamalı Akışkanlar Dinamiği, Akışkan Osilatör, Çarptırmalı Jet Isı Transferi İyileştirme

CONTENTS

M.Sc. THESIS EXAMINATION RESULT FORM ii
ETHICAL DECLARATION iii
ACKNOWLEDGMENTS iv
ABSTRACT v
ÖZ vi
CONTENTS vii
NOMENCLATURE ix
LIST OF TABLES x
LIST OF FIGURES xi

CHAPTER 1 - INTRODUCTION 1
1.1. Literature Review 3
1.2. Objectives and Scope of Work 11

CHAPTER 2 – NUMERICAL METHOD 13
2.1.Problem Definition 13
2.2. Non-dimensional Parameters 14
2.1.1.Reynolds Number 14
2.1.2.Nusselt Number 14
2.1.2.1 Local Nusselt Number 14
2.1.2.2 Average Nusselt Number 15
2.3.Governing Equation 15
2.4.Geometry and Boundary Condition 17
2.5.Mesh Independence 19

CHAPTER 3 – VALIDATION STUDIES 21
3.1 Internal Fluid Dynamic Result 22

3.2 Heat Transfer Result 29

CHAPTER 4 - RESULTS 37

4.1.Effect of Impact Angle 37

4.1.1.Internal Fluid Dynamic Result 38

4.1.1.1.Angle of 30° 38

4.1.1.2.Angle of 45° 41

4.1.1.3.Angle of 60° 45

4.1.2.Heat Transfer Result 49

4.2.Effect of Distance Between Oscillator Outlet Centers 53

CHAPTER 5 –CONCLUSION&DISCUSSION 59

REFERENCES 62

CURRICULUM VITAE 67

NOMENCLATURE

Roman Letter Symbols

A	Characteristic length (m)
L_g	Gap length between two oscillator centers
Nu	Nusselt number
Re	Reynolds number
P	Pressure (Pa)
P_0	Pressure of operating
P*	Non dimensional pressure (P/P_0)
T_f	Oscillating period (s)
T	Temperature (K)
T_i	Temperature of inlet (K)
T*	Non dimensional temperature (T/T_i)
q’	Heat flux (W/m^2)
u	Velocity (m/s)
u_i	Velocity of inlet (m/s)
u*	Non dimensional velocity (u/u_i)

Greek Letter Symbols

ρ	Density (kg/m^3)
α_i	Impact angle
ω	Omega (turbulence equation)

Abbreviations

CFD	Computational Fluid Dynamics
RANS	Reynolds averaged Navier Stokes
SST	Shear Stress Transport

LIST OF TABLES

Table 2.1 Thermo-physical Properties 18
Table 4.1 Table of results for all analyses.....58

LIST OF FIGURES

Figure 1.1 Regions of jet impingement flow [6] 2
Figure 1.2 Wall attachment fluidic oscillator schema [11] 3
Figure 1.3 Section of membrane oxygenator 4
Figure 1.4 Fluidic Oscillator General Working Principles [17] 5
Figure 2.1 The Oscillator Computational Geometry 18
Figure 2.2 Mesh Independence Study 20
Figure 2.3 Mesh Structure Figure 20
Figure 3.1 The Dimensionless Velocity Contour for Half Period at Re=3000 23
Figure 3.2 The Dimensionless Velocity Contour for Half Period at Re=4000 24
Figure 3.3 The Dimensionless Velocity Contour for Half Period at Re=5000 25
Figure 3.4 The Dimensionless Pressure Contour for Half Period at Re=3000 26
Figure 3.5 The Dimensionless Pressure Contour for Half Period at Re=4000 27
Figure 3.6 The Dimensionless Pressure Contour for Half Period at Re=5000 28
Figure 3.7 The Pressure Difference of the Flow at Different Re Numbers 29
Figure 3.8 The Time-averaged Distribution of the Nu Number for the **a)** X/L=0.25 and **b)** X/L=0.5 at Re=3000 30
Figure 3.9 The Time-averaged Distribution of the Nu Number for the a) X/L=0.25 and b) X/L=0.5 at Re=4000 31
Figure 3.10 The Time-averaged Distribution of the Nu Number for the a) X/L=0.25 and b) X/L=0.5 at Re=5000 32
Figure 3.11 Non-dimensional Temperature Contour at Re=3000 33
Figure 3.12 Non-dimensional Temperature Contour at Re=4000 33
Figure 3.13 Non-dimensional Temperature Contour at Re=5000 34
Figure 3.14 The Time-averaged Nu Number Distribution on Impact Surface at Re=3000 35
Figure 3.15 The Time-averaged Nu Number Distribution on Impact Surface at Re=4000 35
Figure 3.16 The Time-averaged Nu Number Distribution on Impact Surface at Re=3000 36
Figure 4.1 The Dimensionless Velocity Contour for Half Period at Re=7000 39
Figure 4.2 The Dimensionless Pressure Contour for Half Period at Re=7000 40

Figure 4.3 The Dimensionless Velocity Contour for Half Period at Re=10000 40
Figure 4.4 The Dimensionless Pressure Contour for Half Period at Re=10000 41
Figure 4.5 The Dimensionless Velocity Contour for Half Period for 45° at Re=4000...42
Figure 4.6 The Dimensionless Pressure Contour for Half Period for 45° at Re=4000...43
Figure 4.7 The Dimensionless Velocity Contour for Half Period for 45° at Re=10000.44
Figure 4.8 The Dimensionless Pressure Contour for Half Period for 45° at Re=10000.44
Figure 4.9 The Dimensionless Velocity Contour for Half Period for 60° at Re=4000...45
Figure 4.10 The Dimensionless Pressure Contour for Half Period for 60° at Re=4000.46
Figure 4.11 The Dimensionless Velocity Contour for Half Period for 60° at Re=10000 47
Figure 4.12 The Dimensionless Pressure Contour for Half Period for 60° at Re=10000 48
Figure 4.13 The Dimensionless Pressure Drop of the Flow at Different Impinging angle with respect to Various Re Numbers 49
Figure 4.14 The Time-averaged Nu Number Distribution on Impact Surface at Re=4000 for a) Angle 30° and b) Angle 60° 50
Figure 4.15 The Time-averaged Nu Number Distribution on Impact Surface at Re=7000 for a) Angle 45° and b) Angle 60° 51
Figure 4.16 The Time-averaged and Area-averaged Nu Number Value 52
Figure 4.17 Non-dimensional Temperature Distribution at Re=10000 for a) Angle 30 and b) Angle 60 53
Figure 4.18 The Dimensionless Pressure Contour 1/2Tf for 8D at Re=7000 54
Figure 4.19 The Dimensionless Pressure Contour 1/2Tf for 7D at Re=7000 55
Figure 4.20 The Time-averaged and Area-averaged Nu Distribution for Various Distance 56
Figure 4.21 The Time-averaged Nu Distribution at X/L=0.25 57

CHAPTER 1

INTRODUCTION

Nowadays, with the development of technology, heat transfer requirements that limit the performance and size of the systems have emerged in many engineering designs. The development of high-thermal performance systems has increased the need for heat transfer improvement methods. Heat transfer enhancement in applications such as electronic equipment cooling, and turbine blade cooling provides the heat transfer rates necessary for the functionality and durability of these systems. Air-cooled heat exchangers, pin fin arrays to have a heat transfer rate of about 100 W/cm^2. [1] This situation has led to the search for various methods to increase heat transfer rates in engineering applications and thus lower the equipment and system temperature.

Heat transfer enhancement methods can be classified as active and passive methods. Passive methods are applications that do not require external power consumption, such as rough surfaces or extended surfaces. [2]On the other hand, active methods require external power input. These are applications such as fluid vibration or jet impingement. [3]

Among all the methods of improving heat transfer, the use of jet impingement has great potential. Impingement jet cooling is a very effective method for cooling equipment and systems operating in high-temperature environments.[4] It can impressive thin the boundary layer, and increase the turbulence in the fluid, thereby increasing the heat transfer capacity. [5] As seen in Figure 1.1 the velocity distribution of the fluid at the jet exit is uniform. The point where the jet stream and the impact surface coincide is called the stagnation point. (Local velocity is zero but static pressure is maximum at this point.) In impingement jets, the flow region is generally divided into three regions: the free jet region, the stagnation region, and the wall jet region. [6] As the flow exits the stagnation zone, it develops as wall jets towards the periphery and slows down in the flow direction. Meanwhile, the boundary layer thickness is gradually increasing. [7]

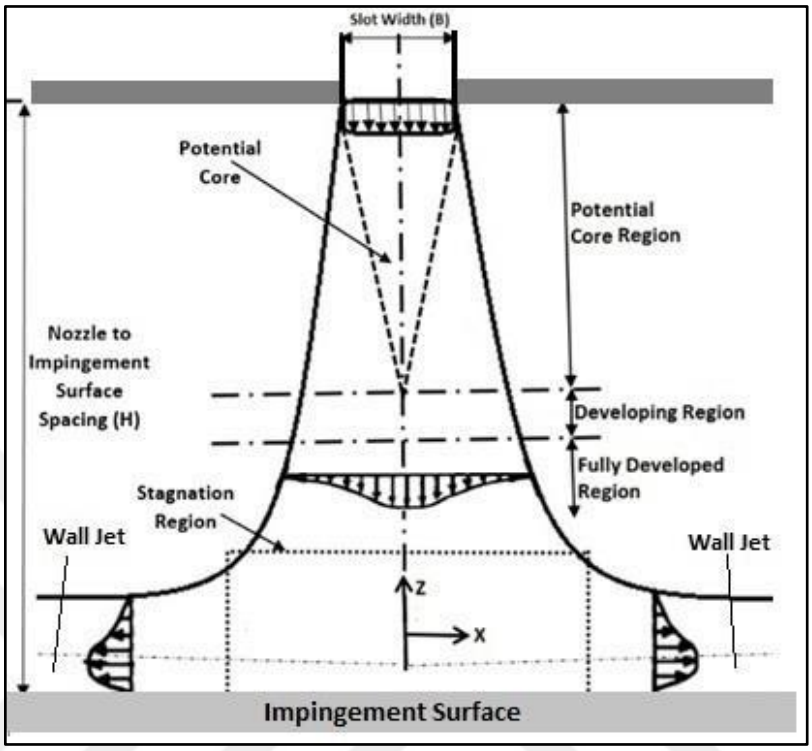

Figure 1.1 Regions of jet impingement flow [6]

In other words, since the Nu number decreases extremely from the stagnation point to the wall, the steady jet impingement can only effectively cool the region it hits. [8] The fluid oscillator is a unique device that converts a steady jet stream without any moving parts into a sweeping jet based on internal instability mechanisms.[9] This sweeping was self-induced and self-sustained. [10] Fluid oscillators are classified into two groups. These are wall attachments and jet interaction oscillators. Wall attachment fluidic oscillators works based on bi-stable attachment mechanisms of a jet to adjacent connecting walls. The most dominant physical phenomenon is the Coanda effect.

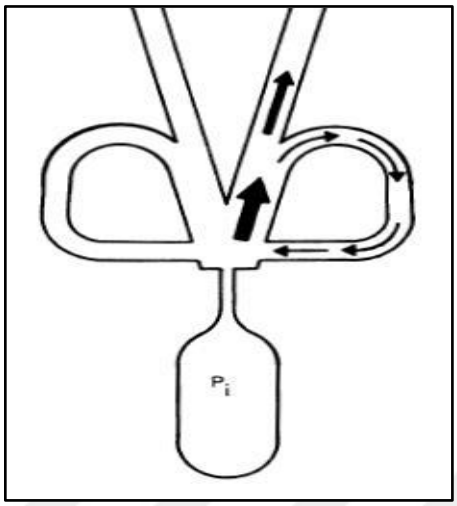

Figure 1.2 Wall attachment fluidic oscillator schema [11]

The Coanda Effect is the result of the sweep of fluid between a jet and a wall and the formation of a low-pressure area that directs the fluid toward the wall. The jet-interaction devices without any attachment walls, such that bi-stable connectivity is not a related mechanism. there are internal feedback paths that trigger instability although there are no attachment walls.[11] Wall attachment type oscillators are divided into three classes: two feedback, single feedback and feedback-free.[12] In this study, two feedback from wall attachment type oscillators were used.

In addition, there are many factors that affect the behavior of the fluid and the amount of heat transfer. These are described in the next chapter.

1.1. Literature Review

Fluidic oscillators are a special type of fluid device that generates a pulsed jet at a wide range of frequencies by a pressurized fluid for active flow control. These originated mainly in the 1960s using only stationary parts for fluidic logic, amplification, sensing, control. [13] Application areas have developed rapidly over time. Fluidic oscillators applications, fluidic amplifiers, combustion, flow separation control and drag reduction, controlling actions, flow meters, mixing or separation of chemical components, micro-

buble and micro-drops generating, noise control, injector nozzles, combustion instabilities suppressing, thrust vectoring, different types of sensors, valves, well drillings, and impinging jet heat/mass transfer enhancement.

One of the first application areas was the use of mass and transfer improvement in a membrane blood oxygenator by a sweeping flow. Oxygenator is one of the life support devices widely used in the health sector. Its main function is to take away carbon dioxide from the blood and to heat transfer among the blood and the wall cell. The diagram of the blood flow pattern is shown in Figure 1.3.

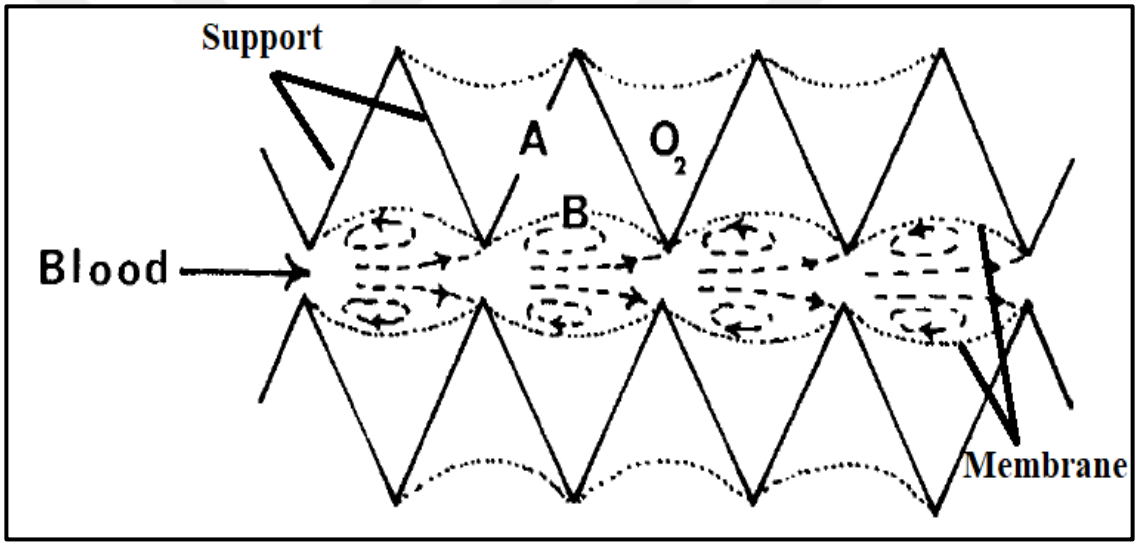

Figure 1.3 Section of membrane oxygenator

As seen in the figure, grooves parallel to the blood flow are used. Blood is pumped into the channel and powerful vortices occur as it passes over the grooves. When the flow backs, the vortices are removed from the troughs where counter-rotating vortices are formed. In this way, mass transfer and heat transfer are improvement. [14]

In heat transfer and mass transfer improvement studies, one of the commonly used techniques is steady impinging jet, in addition to the groove and communicating flow techniques placed in the channel. Gardon and Cobonpue [15] found the rate of heat transfer to the jet flow, which varies from point to point at the impact surface, depending

on the difference between the impinging wall temperature and adiabatic wall temperature. Gardon and Akfirat [16] determine that the increase in turbulence in the jet has a significant effect on the heat transfer between the impact surface and the jet. The disadvantage of the steady jet impingement flow is that the Nusselt number increases heat transfer in a small region, but the Nusselt number decreases abruptly with the expansion of the flow at the impinging surface. Sweeping the jet flow increases heat transfer as it will increase the turbulence in the jet and dissipate the stagnation point. Fluid oscillators are the most suitable device for sweeping flow. The working principles of fluid oscillators are pretty simple. They do not contain any moving parts, therefore both production costs and maintenance are low Figure 1.4 depicted the schematic of a wall-attachment fluidic oscillator and its working principle.

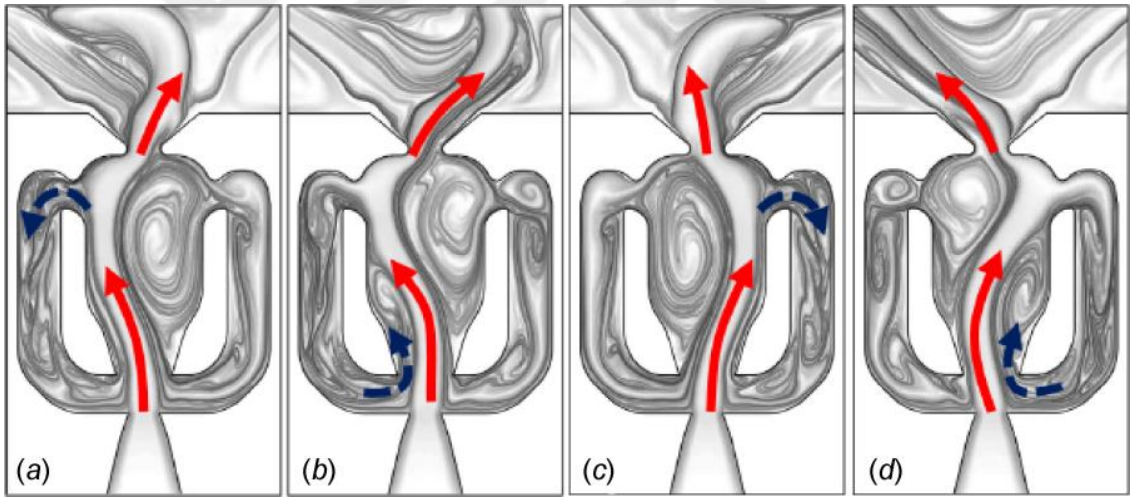

Figure 1.4 Fluidic Oscillator General Working Principles [17]

A jet flows into the cavity through a pressurized channel through the power nozzle. The jet expands to fill the throat and feedback channels. It is more effective if two opposite vortices occur on either side of the power jet. As the intensity of the vortices increases, a vortex becomes dominant. This causes the jet flow to be diverted to the opposite wall due to the pressure difference. When the power jet is directed to the side wall, it sticks to the wall due to the “Coanda Effect”. This allows some of the fluid to enter the feedback loop,

which flows back into the control port and causes the power jet to separate from the sidewall. The power jet then passes to the opposite supply wall, and a similar process results in an oscillating fluid motion at the outlet of the throat. [18]

Although fluidic oscillator was used in many fields, the properties of internal fluid dynamics characteristics such as pressure difference, oscillation frequency etc. have not been fully investigated. Seo et al. [19] performed CFD analyzes on some parameters to see the effect of geometric properties in a fluid oscillator with two feedback channels. In the study, first of all, the oscillation frequency of the flow and the pressure differences occurring in the feedback channel during the oscillation were determined. Then the feedback channel length was modeled as 1D (baseline), 2D, and 3D to see the effect of geometric changes. In addition, while the feedback channel length was 1D, the mixing chamber length was modeled as 4.5D, 4.75D, 5D, and 5.25D. As a result of the study, it has been observed that the length of the feedback channel has no effect on the jet frequency, but the oscillation amplitude decreases slightly as the channel length increases. It is concluded that there is a non-linear inverse relationship between chamber length and frequency.

Hossain et al. [20] experiments and CFD analyzes were performed to observe the effect of surface roughness on the performance of the fluidic oscillator. Two different sandpapers with 25.28 μm and 46.54 μm surface roughness were used to increase the surface roughness in the experiments. As a result of the experiments and analyzes, it was observed that the increase roughness in the throat region (the effective aspect ratio in the throat region increases) get bigger the oscillation frequency at low mass flow rates. It is observed that increasing roughness in the chamber and feedback channel negatively affects the performance of the fluidic oscillator and reduces the oscillation frequency by creating additional blocking.

Tomac and Gregory [21] performed tests with a 1300 Reynolds Number feedback-free fluidic oscillator using the PIV technique. Two jet inlets were used in the test mechanism and it was observed that these jets collided with each other. As a result of these collisions,

it was determined that four main eddies were formed. Two of them were called domes and two of them were called side vortices. It was observed that these two eddies caused the bifurcation that occurred after the collision of two jets. While it was determined that these vortices disappeared in the process, it was observed that the side vortices never disappear, only their size and strength changed. Uzol and Camci [22] studied the mechanism by which the jet flow from the oscillator impinges on a chamber with concave surface. They observed that the jet began oscillate through the chamber as the eddies get stronger and their size changes. They observed that the frequency changes linearly with the Reynolds number, but after the Reynolds number exceeds 1000, they found that the Strouhal Number remains almost constant at 0.007. Bobusch et al. [23] accomplished a parametric work on geometric features such as outlet nozzle area, mixing chamber inlet wedges, and feedback channel geometry. It was observed that the oscillation frequency and deviation angle did not change with the change of the outlet nozzle area. Although, there was no increase in mass flow with the change of the outlet area, it was observed that the change in the area changed the outlet velocity. In this study, it was found that the frequency mainly depends on how fast the jet flow is transported from the feedback channel to the separation bubble. It was also observed that the decrease in the wedge distance creates additional resistance at the inlet, thus negatively affecting the frequency.

In addition to investigating the factors affecting the performance of the oscillator, the use of oscillators to increase system performance has been examined in many different disciplines in the open literature. These can be given as examples of work areas such as flow separation control, heat transfer improvement, thrust vectoring, and drag reduction.

The fluidic oscillator was widely used in flow separation control. Woszidlo et al. [24] studied the use of a fluidic oscillator array to control flow separation on the Multiple Flap Airfoil (MFA). It was observed that the oscillation occurred at high frequency in direct proportion to the volumetric flow rate. It was determined that the distance between the oscillators array depends on the ratio of jet flow and free stream velocity. Since there are many parameters for optimization within the scope of this study, the effect of temperature, pressure, oscillation frequency, density boundary layer effect and free flow instability of

air did not consider in this study. Reducing friction is a very important issue in the automotive industry as it is in aviation. Gregory and Metka [25] carried out experimental work on drag reduction by disrupting the unstable wakes formed behind the vehicle with the jet flow coming out of the fluidic oscillator. By eliminating the separation bubble formed on the rear inclined surface of the vehicle, it was observed that the external flow was delayed from breaking off from the vehicle surface and drag was reduced by %7.5. It is stated that this method can be applied at low speeds and with the energy applied to the operate the fluidic oscillator, a maximum of 5% energy is saved. Finally, it was also observed that the drag coefficient depends on the separation bubble size and strength and the radius of curvature of the back surface.

Choephel et al. [26] performed experiments and numerical studies to observe how using a fluidic oscillator to improve wing profile aerodynamic performance. According to the results of the study, it was determined that the lift coefficient improved between %10-20 with the use of the fluidic oscillator. In addition, it was observed that the lift coefficient increased with increasing jet speed up to a certain Reynolds Number. An important results of the study is that when the ratio of jet velocity to free flow velocity is kept constant, the improvement in lift remains almost constant despite varying Reynolds numbers.

Lin et al. [27] aimed to increase the side force by 20% with 37 two feedback fluidic oscillators placed on the hinge of the vertical tail of Boeing 757 aircraft. The test were carried out in a wind tunnel at the NASA Ames Research Center at a nominal seed of 100 knots (Ma~0.15, Re~15 million) at a maximum rudder angle of 30° and side slip angles of 0° and -7.5°. The fluidic oscillator were not all operated at the same time. With the 18 fluidic oscillators in operation, the targeted %20 side force increase was almost achieved. However, considering all the cases, it was stated that 31 oscillators should be used to reach the targets. The successful conclusion of the tests was inspiring for the future use of fluidic oscillators in flight. Phillips et al.[28] observed the effects of unsteady flow on the trailing edge flap and the effect on the airfoil as the lift, drag, and pitch angles change rapidly. With the fluidic oscillator, it is aimed to increase the wing's transition angle to the stall and to increase the lift force significantly. As a result of the experiments, flow separation

is prevented at high angles of attack and flap deviations with the use of a sweeping jet, it is observed that the drag coefficient decreased by 3 times while the maximum lift force is doubled.

Separation control on the airfoil is very important to increase efficiency in the field of wind turbines as well as in aviation. Cerretelli et al. [29] tested a fluidic oscillator with two feedback channels for separation control in a wind turbine airfoil for the Reynolds Number range of $2\times10^6 \leq Re \leq 4.8\times10^6$. While an increase of %10-60 is observed in the lift coefficient value depending on the Reynolds Number, it is observed that the boundary layer thickness decreased dramatically and increased turbulence.

Thrust vectoring is very important in flying the aircraft along the desired route or in obtaining the required moment of attitude control in the aircraft. There are two traditional methods of providing thrust vectoring. Turning the entire jet exit area in the desired direction or using secondary flow to direct jet to the desired course. Raman et al. [30] developed a new approach to thrust vectoring using a microfluidic oscillator. While the experiments are carried out at subsonic speed, the oscillator nozzle throat is operated at pressure of 20.68 kPa and 165.47 kPa. There are two important outputs of this study, the first is that the jet can be directed to the desired direction when a single fluidic oscillator device is used, and the second is that when two fluidic oscillator devices are used, a 28% mass flux increase is observed with the flow direction. Based on these studies, it has been suggested that fluidic oscillators can be used in fluid deflection applications.

Combustion instabilities in high-performance combustion systems are caused by pressure swings caused by heat releases. Sweeping jet, which is one of the active control methods, is used to disrupt combustion instabilities. [31] Guyot et al. [32] performed experimental studies to demonstrate the performance of the fluidic oscillator in an active combustion control system. Two different burners and a fluidic oscillator with one inlet and two outlets were used in the tests. It is observed that the oscillation frequency reached up to 220 Hz by changing the input mass flow. Water, natural gas, nitrogen and natural gas-nitrogen mixture are used in the tests.

Many studies have been carried out to investigation the heat transfer performance by sweeping the flow. Camci and Herr [2] first time used an fluidic oscillator to transform the jet stream into a self-sustained impingement jet to improve the heat transfer performance of impinging jets. Air is used as the fluid and Reynolds Numbers 7000, 10000, and 14000 are used in the tests. With the impact of the impinging jet on the larger impinging area due to its oscillating motion, an increase in heat transfer performance between 20%, and 70% is observed compared to the fixed jet values. Kim et al.[33] experimentally studied the heat transfer of oscillating jet impinging a flat wall for 3600, 6400, 11000, and 15300 Reynolds Numbers and several nozzle-wall spacing. It is showed that the heat transfer of the sweeping jet augmented compared to a steady flow of jet. Hossain et al.[34] performed a numerical study to observe the effect of the curvature of the impact surface on the heat transfer performance of the swept jet flow.

In the study carried out on a feedback fluidic oscillator with three different aspect ratios, it was observed that the heat transfer increased as the surface curvature increased. However, this increase is not continuous and it was observed that the heat transfer decreased dramatically after a certain curvature diameter. It was determined that the highest Nu distribution was in the case where the radius of curvature was 20 D_h. Kim et al.[35] two feedback fluidic oscillators are investigated numerically and experimentally by passing the working fluid through the constant temperature channel wall. As a result of the study, it has been shown that the non-dimensional (St Number) sweeping frequency is independent of the working fluid type and mass flow rates. In addition, it is observed that the frequency increased as the Re Number increased, but the heat transfer in the channel did not change significantly. It has been stated that reason for this is the increase in the convection velocity of the eddies with increasing mass flow rate.

Ghanami and Farhadi[36] carried out experiments with three different types of oscillators: no feedback, single feedback, and double feedback, to observe the heat transfer effect of the fluidic oscillator on a single tube heat exchanger. While constant heat flux and constant periodic discontinuous heat flux were given to the tube surfaces, the Reynolds Number was taken as 5600-16400. The highest heat transfer improvement rate was 83% in the

double feedback fluidic oscillator, while 37% enhancement was observed in the single feedback, and 23% in the feedback-free. Hossain et al.[37] performed numerical analyzes to observe the effect of steady stream jet and oscillating jet on heat transfer enhancement on a flat plate at 3, 4, 6 and 8 hydraulic diameter jet-plate spacings for five different mass flow rates. It was observed that the sweeping jet is better in improving heat transfer than steady stream jet, while the enhancement performance decreased with the increase of the distance.

Mataoui et al.[38] heat transfer by forced convection of a jet impinging on a hot rectangular space is investigated by numerical analysis. Depending on the position of the jet outlet in the cavity, different flow forms occur and its effect on heat transfer is investigated. The three walls of the cavity are simultaneously cooled by the oscillation of the jet, and the heat transfer in the cavity walls is periodic. As a result of the study, it is determined that the position of the maximum Nu number changes depending on time. O'Donovan and Murray et al.[39] the effect of the angle of an obliquely impinging air jet and the distance from the impact surface on heat transfer has been investigated experimentally. When the Reynolds Number is 10000, the distance from the impact wall to the jet is 2D and 8D, and the impact angle is between 30 and 90 degrees. It is shown that the maximum Nu number occurs at the stagnation point for oblique impact angles. According to the test result, when the distance to the impact wall is minimum and the impact angle is the lowest, maximum Nu distribution is observed. However, when the distance to the impact wall is maximum and the impact angle is greatest, the maximum Nu distribution is observed.

1.2. Objectives and Scope of Work

The present study focuses on the improvement in heat transfer using a fluidic oscillating jet in a micro-channel heat exchanger. Fluidic oscillators are self-sustaining, do not need any moving parts, and are highly effective tools for augmentation momentum and heat transfer in unstable flows. Nowadays, it is used in many areas such as automotive, aviation, health etc. In recent years, its use has intensified in areas with impingement

cooling. Developing technology led to the formation of systems with high heat load and heat exchanger capacities were insufficient. Thus, compact heat exchangers appeared. There are previous studies on using oscillating flow to increase the convection heat transfer capacity of the coolant in heat exchangers. However, the angle between these oscillators and the channel, the distance between the exit nozzle centers have been not studied. The aim of this study is to examine the effect of an unstable free-flow aerodynamics on the heat transfer performance of the impingement angle with the channel and the distance between the oscillators.

The present study consists of 5 main parts. Chapter 2 includes the problem definition, and discusses the Navier-Stokes equations used in numerical analysis. It also includes boundary conditions and assumed assumptions. In Chapter 3, it contains for 3 different Reynolds Numbers to validate the reference work. Chapter 4 includes the results of the analysis at different impact angles and different oscillator distances with the model which methodology was verified. In the last section, improvements in heat transfer are evaluated.

CHAPTER 2

NUMERICAL METHOD

In this title, the calculation methodology, the definition of the problem, dimensionless parameters, geometric properties, governing equations used in numerical solution, and the mesh properties are introduced. In addition, boundary conditions, assumed assumptions and mesh independence study are explained.

In this simulation, ANSYS FLUENT 21.2's unsteady computation utilized the SIMPLE model for pressure-velocity coupling and the Gauss-Green method for pressure discretization. The second-order upwind method was used for discretization of all parameters to guarantee numerical stability. The time step was determined to be 10^{-5} seconds based on the average velocity at the nozzle throat, where the average flow velocity is high. The simulations were conducted until the oscillation reached a stable state. A convergence criterion of 10^{-5} was adopted for the energy equation, and a criterion of 10^{-7} was adopted for the other equations. The k-ω SST model was employed due to its demonstrated robustness and accuracy in predicting flow behavior, particularly in the vicinity of walls and in high turbulent flow, as determined through the use of the k-ε model.

2.1.Problem Definition

In this study, the phenomenon of convective heat transfer between the coolant, which is introduced through a fluidic oscillator, and the hot wall in a microchannel heat exchanger was observed. The occurrence of forced convection was attributed to the interaction between the impinging jet stream and the hot wall. As the constant jet stream generates a stagnation point that results in a maximal Nu number only at that point, an attempt was made to resolve the problem by oscillating the flow. The direction of gravitational

acceleration was calculated to be a combination of the -z and +x directions, based on the angle it forms with the channel, with the reference point positioned at the inlet.

2.2. Non-dimensional Parameters

Non-dimensional numbers decrease the number of variables of a system, thereby reducing the amount of data needed to make correlations between physical phenomena and systems. [40] In addition, physical parameters are non-dimensionalized to fully understand the consequence of the effects of these occurrences. There are several dimensionless parameters used to express thermo-fluid relationships listed below.

2.1.1. Reynolds Number

The Reynolds number is a dimensionless quantity that describes the ratio of inertial forces to viscous forces in a fluid flow. Reynolds number is commonly used to understand characteristics of the flow and determine the transition from laminar to turbulent flow. The Re number is defined as,

$$\mathrm{Re} = \frac{\rho V D}{\mu} \tag{2.1}$$

Where ρ is the fluid density, V is the fluid velocity, D is characteristic length scale of the flow (such as the diameter of a pipe) and μ is the dynamic viscosity of the fluid.

2.1.2. Nusselt Number

Nusselt number shows the ratio of convective heat transfer with conduction heat transfer with conduction heat transfer inside the fluid at the bounding surfaces where heat transfer is observed.

2.1.2.1 Local Nusselt Number

Local Nusselt number describes the local rate of convective heat transfer between a fluid and a solid surface. The local Nu number can vary significantly along the surface,

depending on the flow conditions, geometry, and thermal properties of the fluid and solid. The local Nu number is represented as

$$Nu_x = \frac{h_x D}{k} \tag{2.2}$$

2.1.2.2 Average Nusselt Number

Average Nusselt number represents the integration of local Nusselt Number for a given surface. It is also used in analytical models and correlations to predict the convective heat transfer coefficient for different flow regimes and geometries. The average Nu number is defined as

$$\overline{Nu} = \frac{1}{D}\int_0^D Nu_x(x)dx \tag{2.3}$$

2.3.Governing Equation

This section of the report will outline the specifications for the boundary conditions of the channel geometry that require verification, the solution method, and the equations that need to be solved. The fundamental equations that need to be solved in the study are the conservation of mass, momentum, and energy equations. In addition, the turbulence model equations will be incorporated to account for the turbulent flow nature. The preferred turbulence model for solving the flow problem in the channel is k-ω SST, which provides more accurate results in pipe and channel flows compared to other turbulence models. Therefore, this study uses the k-ω SST turbulence model for more reliable results.

For incompressible fluid flows in the microchannel, the **continuity equation** is

$$\frac{\partial(\rho u_i)}{\partial x_i} = 0 \tag{2.4}$$

The mass conservation equation, which describes how the rate of change of mass in a fluid elements is equal to the net rate of mass flow in or out of the element through its surface. Another important governing equation is the momentum equation, which explains how forces acting on an object affect its motion. By using the decomposition and time averaged equation, it is obtained as follows,

Momentum Equation

$$\frac{\partial(u_i)}{\partial t}+\frac{\partial(u_i u_j)}{\partial x_j}=\frac{-1}{\rho}\frac{\partial P}{\partial x_i}+\frac{\partial}{\partial x_j}\left(\nu\frac{\partial u_i}{\partial x_j}-\overline{u_i' u_j'}\right) \quad \textbf{(2.5)}$$

where $\overline{u_i' u_j'}$ represent to turbulent fluctuating.

Energy Equation

$$\frac{\partial(\rho c_p T)}{\partial t}+\frac{\partial(\rho c_p u_j T)}{\partial x_j})=\frac{\partial(\lambda\frac{\partial T}{\partial x_j}-\rho c_p\overline{u'_j T'})}{\partial x_j} \quad \textbf{(2.6)}$$

The k Equation

$$\frac{\partial(\rho k)}{\partial t}+\frac{\partial(\rho k u_j)}{\partial x_j})=\frac{\partial(\Gamma_k\frac{\partial k}{\partial x_j})}{\partial x_j}+G_k-Y_k+S_k+G_b \quad \textbf{(2.7)}$$

The ω Equation

$$\frac{\partial(\rho\omega)}{\partial t}+\frac{\partial(\rho\omega u_j)}{\partial x_j})=\frac{\partial(\Gamma_w\frac{\partial\omega}{\partial x_j})}{\partial x_j}+G_\omega-Y_\omega+S_\omega+G_{\omega b} \quad \textbf{(2.8)}$$

The variable G_k and G_ω represent the generation of turbulent kinetic energy due to the average velocity gradients, while Γ_k and Γ_w symbolize the effective diffusivity of k and ω, respectively. Y_k and Y_ω represent the dissipation due to turbulence, and S_k and S_ω are user defined source terms. The terms G_b and G_w also account for buoyancy effects on turbulence.

2.4.Geometry and Boundary Condition

This study investigates the effects of angled two feedback fluidic oscillators on heat exchanger channels at an angle of α_i, with a gap of L_g between them. The numerical setup involved examining the effect of the angle of the oscillator input surface with respect to the channel (α_i) at three different values: 30°, 45°, and 60°. Additionally, the distance between the exit surfaces is varied and analyzed at three different distances (L_g): 7D, 7.5D, and 8D. The fluidic oscillators have a power nozzle, mixing chamber, two feedback channels, outlet throat, and exit hole with a trailing edge of 4 D. The dimensions of the fluidic oscillator are 0.5 D thickness and D height. The nozzle entrance extends forward and parallel to the impact surface with a minimum width of 0.7 D. The outlet of the channel is placed 24 D away from the center of the strait to ensure fully developed flow and minimize the impact of the outlet boundary condition on the fluid dynamics of the oscillating jets. The inlet of the power nozzle is 2D, wide, and its minimum width is 0.7D at a distance of 2.65 D from the inlet. The mixing region inlet in the feedback channel has a width of D. Figure 2.1 provides the computational model's specifics.

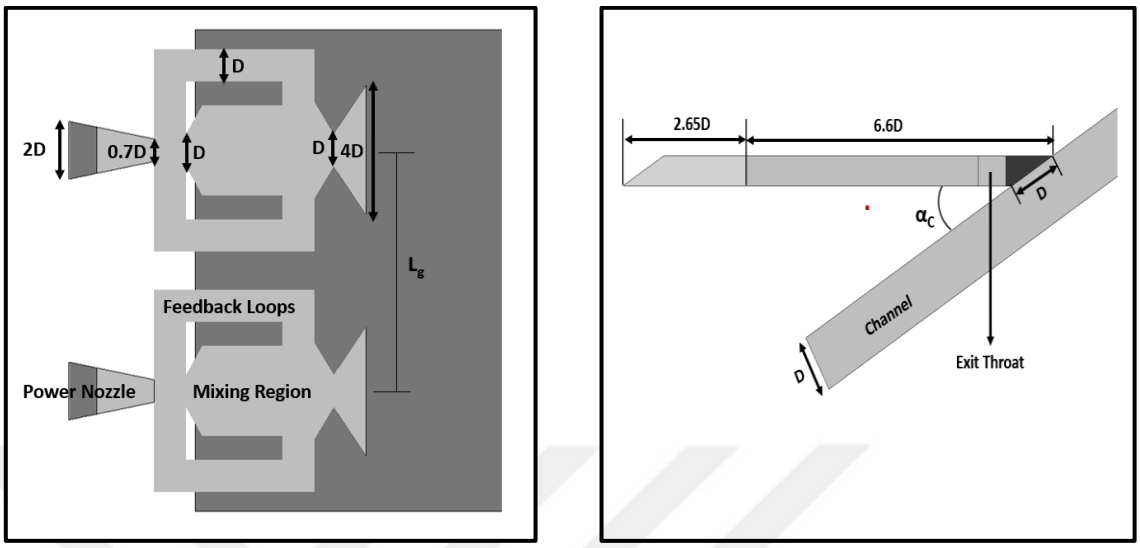

Figure 2.1 The Oscillator Computational Geometry

The numerical investigation employed water as the working fluid, which was selected based on its widespread use and availability. In this study assumes that the fluid entering the model is uniform and has a temperature of 300 K. The thermos-physical properties of water at the inlet temperature were considered, and the corresponding values are presented in the Table 2.1.

Table 2.1 Thermo-physical Properties

Density	Viscosity	Specific Heat	Thermal Conductivity
997	0.000855	4178	0.615

The outlet pressure, located 24 D away, is set to 0 Pa to prevent any impact on the flow area. For model validation, the Re Number ranges from 3000 to 5000, while parametric studies are conducted using 4000, 7000, and 10000. The channel's impingement surface has constant heat flux boundary condition of $q'=10^6$ W/m^2, while the other walls in the model are considered adiabatic and non-slip. The impingement surface, measuring 9D × 15D, is modeled as a hot wall.

2.5.Mesh Independence

Mesh independence study is a method used in a numerical simulations to evaluate the impact of mesh size or resolution on the accuracy of the results obtained from the simulation. In CFD, for instance, the solution of the governing equations is computed on a discrete mesh or grid, and the accuracy of the solution depends on the resolution of the mesh. To conduct a mesh independence study, the simulation is run multiple times using different mesh sizes or resolutions. The results are then compared to determine if there is a significant difference between them. If the results vary significantly with changes in mesh size, then the simulation is considered to be dependent on the mesh size and the mesh needs to be refined to obtain more accurate results. On the other hand, if the results are relatively insensitive to changes in mesh size, then the simulation is considered to be mesh independent.

The goal of a mesh independence study is to determine the minimum mesh resolution required to achieve accurate results while minimizing computational cost. This is particularly important in cases where the computational cost of a simulation is high, as in many engineering applications, where simulations can take several hour or even days to complete.

In this study, the significance of the mesh independence study is underscored by the time-dependent nature of the analysis and the prolonged duration of a single case, which can span several days. In the analysis, three distinct mesh types were utilized, denoted as coarse, medium and fine, with corresponding node counts of 3350874, 6849175, and 8329482 respectively. To ascertain the mesh independence of the obtained results for a given Re number (5000), a mesh independence study was performed, involving the analysis of frequency data for the three mesh sizes. Specifically, the computed frequency values for the coarse, medium and fine meshes were 122, 126, and 127 respectively. Notably, the frequency value in the reference study differed slightly from the error rate in the results derived from the medium and fine meshes by less thang 2%, suggesting the mesh independence. As such, the choice of mesh size was deemed not to significantly

affect the outcomes, leading to the adoption of the medium mesh with reduced number of nodes.

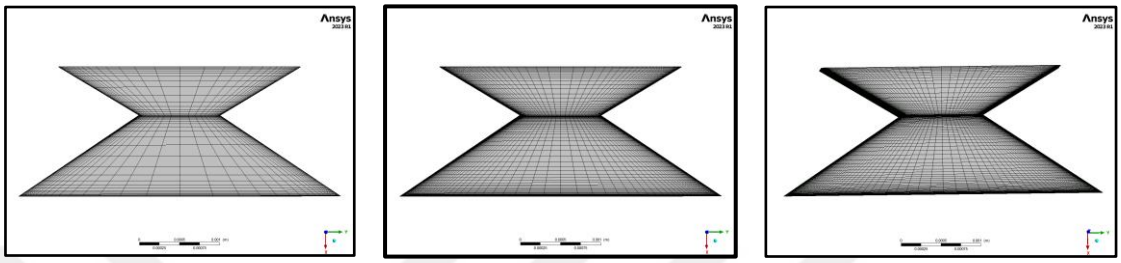

a) Coarse Mesh b) Medium Mesh c) Fine Mesh

Figure 2.2 Mesh Independence Study

The mesh model used in the analysis is illustrated in Figure. During the meshing process, a bias factor was applied to achieve y+ ~1 on the walls, and a finer mesh was used in the power nozzle and throat regions. This ensured an accurate capture of the boundary layer and reduced the possibility of numerical errors. The mesh was also refined the impact wall to accurately capture the flow behavior in those regions.

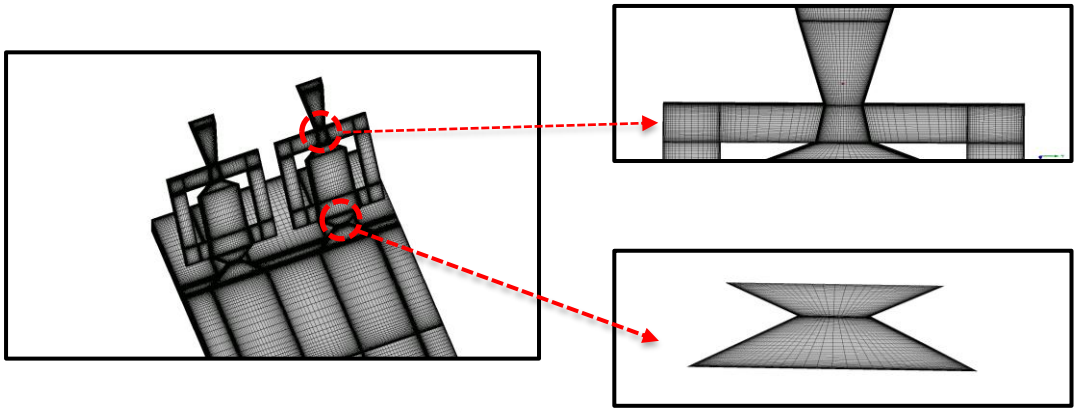

Figure 2.3 Mesh Structure Figure

CHAPTER 3

VALIDATION STUDIES

In fluid mechanics, there are two primary methods used to solve problems: testing and calculation. In the past, testing was obligatory due to the limitations of calculation methods, as equations of fluid motion could not be solved. This required setting up certain test environments, such as wind tunnels, and preparing and testing models. However, producing and re-testing a system of new dimensions to evaluate results was a time-consuming and costly process if desired results were not obtained. With the advancement of technology and computational methods, the majority of flow problems in designed systems are solved using computational methods. The process of solving flow problems through calculation is known as Computational Fluid Dynamics (CFD), which is frequently used today to validate engineering problems solved with CFD analysis and to match calculation and test methods.

Fluidic oscillators, which use fluid dynamics principles to generate oscillating flow, are widely used in engineering applications such as flow control, mixing, and heat transfer enhancement. In a time-based study of fluidic oscillators, researchers measure the frequency and amplitude of oscillations over tie and analyze how these parameters are affected by different operating conditions such as flow rate, pressure and geometry. Validating the results of the study is a critical step in ensuring accuracy and reliability. To validate the results, it is important to compare them with experimental data or numerical simulations and evaluate uncertainties and sources of error associated with the measurements. The validation process may also involve performing additional experiments or simulations under different conditions to test the robustness of the results or using statistical methods to measure confidence intervals and correlations between variables. By rigorously validating the time-based work on fluidic oscillators, researchers can ensure that their findings are reliable and can guide the design and optimization of fluid oscillator-based systems.

In this study, based on the Wu Y. et al. study, validation study was carried out and the validity of the model was ensured. In the validation study, only the k-ω turbulence model and the values in the 3000-5000 Re range were examined and the model was validated. The results of this study were collected under two headings as internal fluid dynamic and heat transfer results.

3.1 Internal Fluid Dynamic Result

In this study, the occurrence of a quasi-constant oscillating flow pattern in fluidic oscillators was examined. While the initial flow pattern in the oscillators was random, as the flow passed through the oscillators, asynchronous output phases were observed. Accurately capturing the acceleration of the flow and temporal evolution of the pressure and flow fields within the array as the flow passed through the oscillators was deemed essential.

To investigate the flow patterns, a numerical model was used and compared with a reference study. The results of this study were found to be consistent with the reference study. Figure 3.1 depicts an oscillating flow pattern for the fluidic oscillator, with velocity contours partitioned into six-time increments for one oscillation cycle.

The finding of the study suggests that, for half of the oscillation period at a Re Number of 3000, the interaction between the incoming flows and the main jet in the inlet region causes a deflection of the jet due to the pressure difference in the two feedback channels. At time zero, the fluid adhered to the right wall of the nozzle of the firs oscillator, while it was attached to the left wall of the nozzle of the second oscillator. Additionally, a portion of the fluid was directed towards the feedback channel and returned to the inlet of the oscillator. The study observed that a bubble disappeared as it entered the feedback channel and exited through the outlet. This process was repeated on the opposite wall, resulting in self-sustaining sweeping.

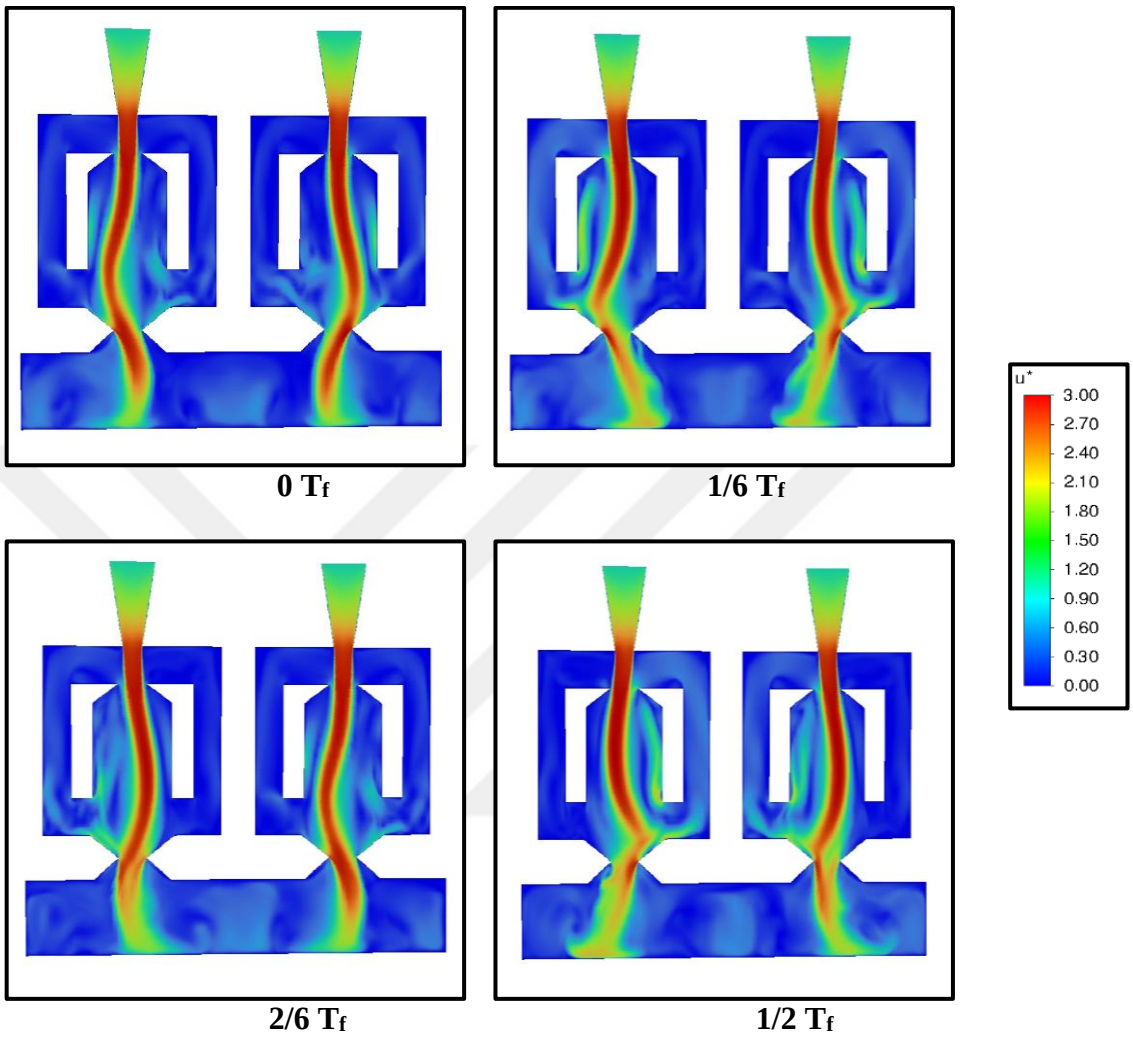

Figure 3.1 The Dimensionless Velocity Contour for Half Period at Re=3000

As the velocity at the inlet of the fluidic oscillator increases, many changes can occur in the channel. Increasing the velocity of the inlet fluid causes an increase in fluid pressure and oscillation frequency. The oscillation amplitude of the fluidic oscillator can also vary. According to Figure 3.2 for Re 4000, the flow pattern in the channel is more turbulent, and larger eddies are formed as the velocity at the inlet of the fluidic oscillator increases. However, it should be noted that these changes in the channel are complex and depend on a variety of factors, such as the dimensions of the chamber, the number and shape of obstructions, and the viscosity of the fluid.

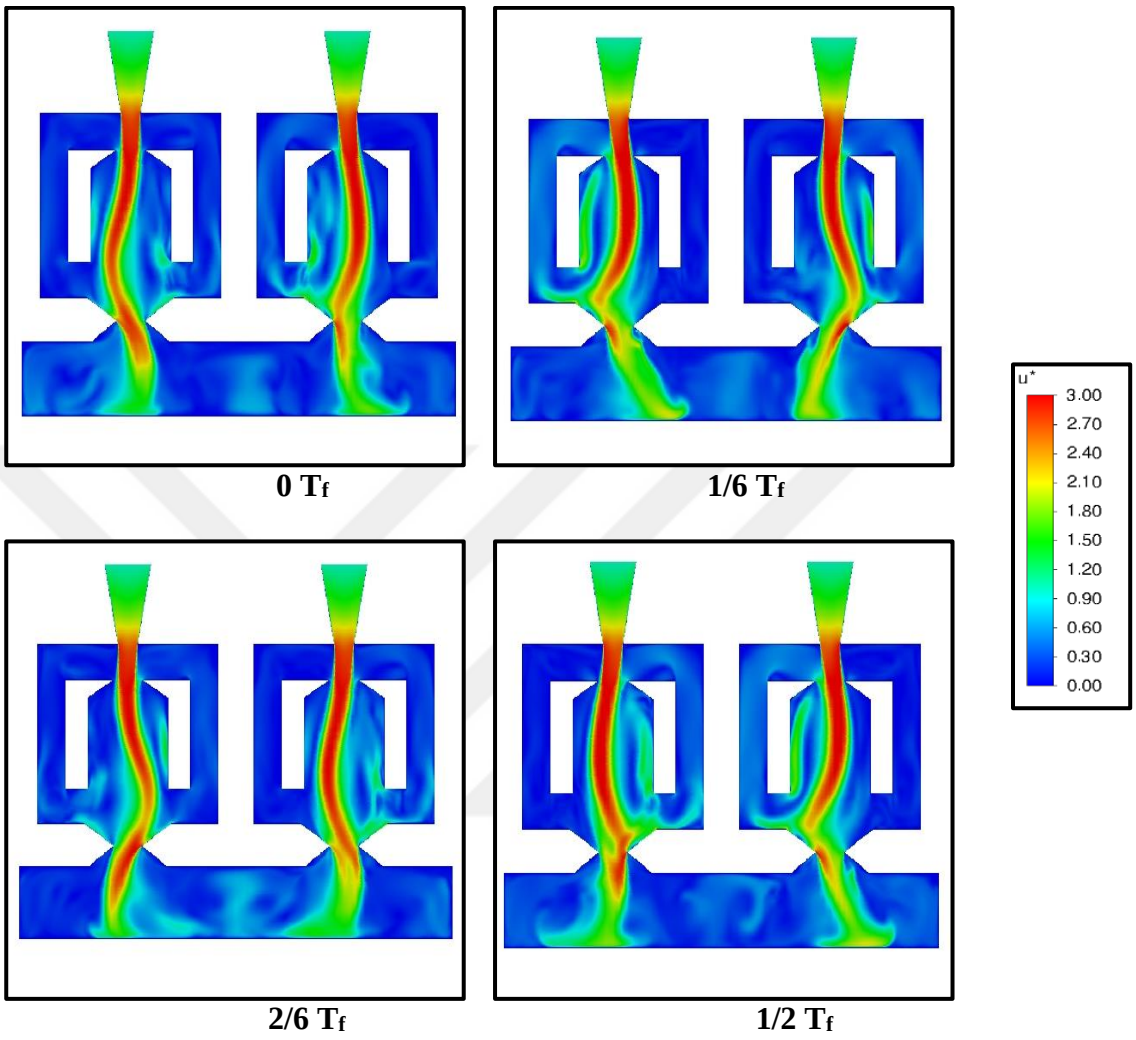

Figure 3.2 The Dimensionless Velocity Contour for Half Period at Re=4000

As Re increases the velocity gradients of the oscillation become steeper, resulting in a more complex and turbulent flow. This is due to the increased inertia of the fluid and the greater influence of the oscillation on the flow. At low Re numbers, the fluid relatively slow and viscous, leading to laminar flow and smoother velocity gradients. However, as Re increases, the flow becomes more turbulent, and the velocity gradients become more uneven, leading to larger vortices and increased mixing.

When the results in the Figure 3.3 for the Re 5000 are examined, it is seen that the flow becomes more complex, although the dimensionless velocity values do not increase which is due to the ration of this velocity to the input velocity.

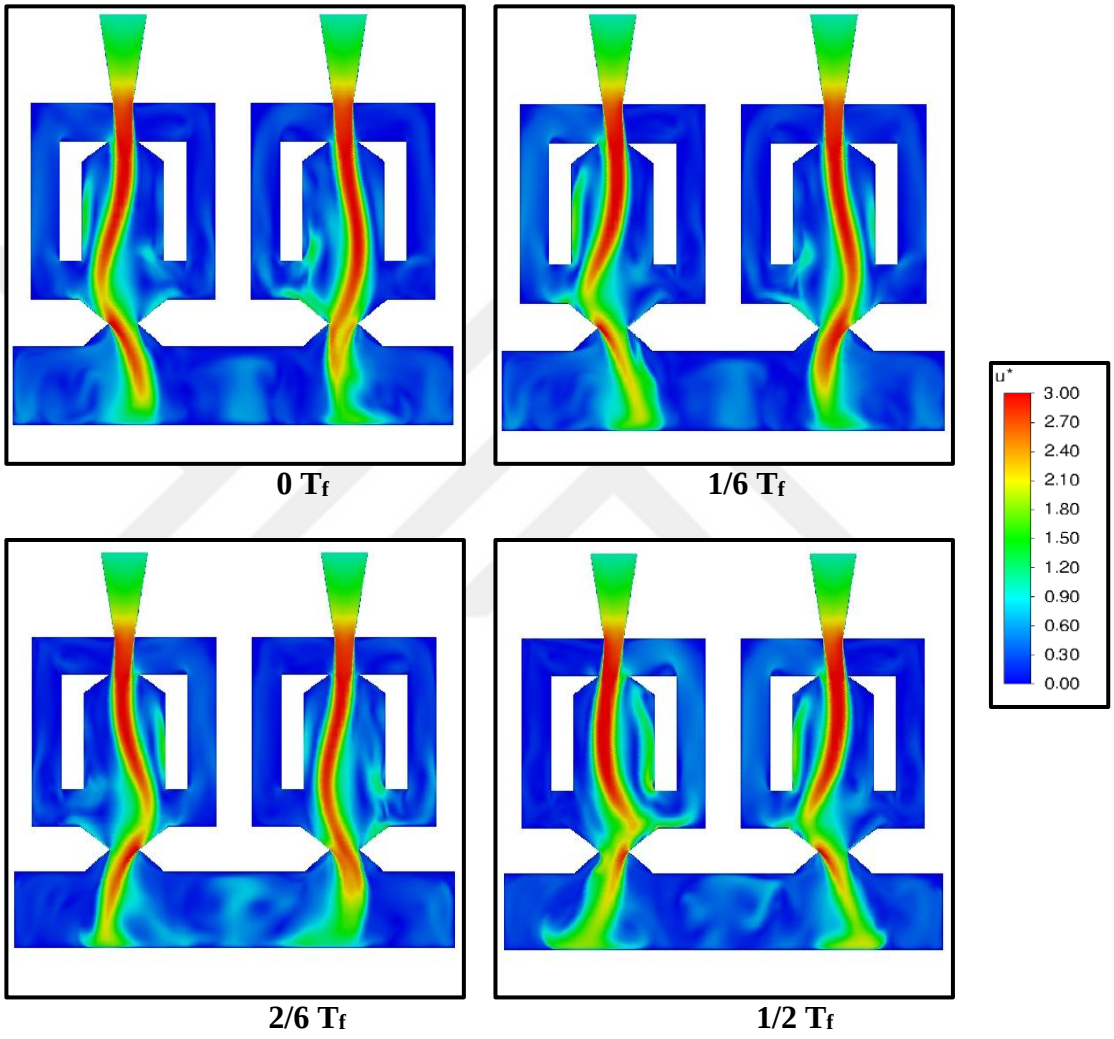

Figure 3.3 The Dimensionless Velocity Contour for Half Period at Re=5000

The dimensionless pressure distribution shown in Figure 3.4 provides evidence of a similar process. When the jet stream attaches to right side of the nozzle wall, it creates high-pressure region in the left feedback channel, which is due to the compression of fluid molecules against the wall. Meanwhile, the flow separation that occurs due to the jet stream's impact on the mixing chamber results in the formation of a bubble and the

generation of negative pressure on the right side of the chamber. This negative pressure is the result of a low-pressure zone that develops due to the abrupt change in flow direction. The observed pressure distribution can be explained by considering the balance between the inertial and viscous forces acting on the fluid, which leads to a complex flow pattern with regions of high and low pressure.

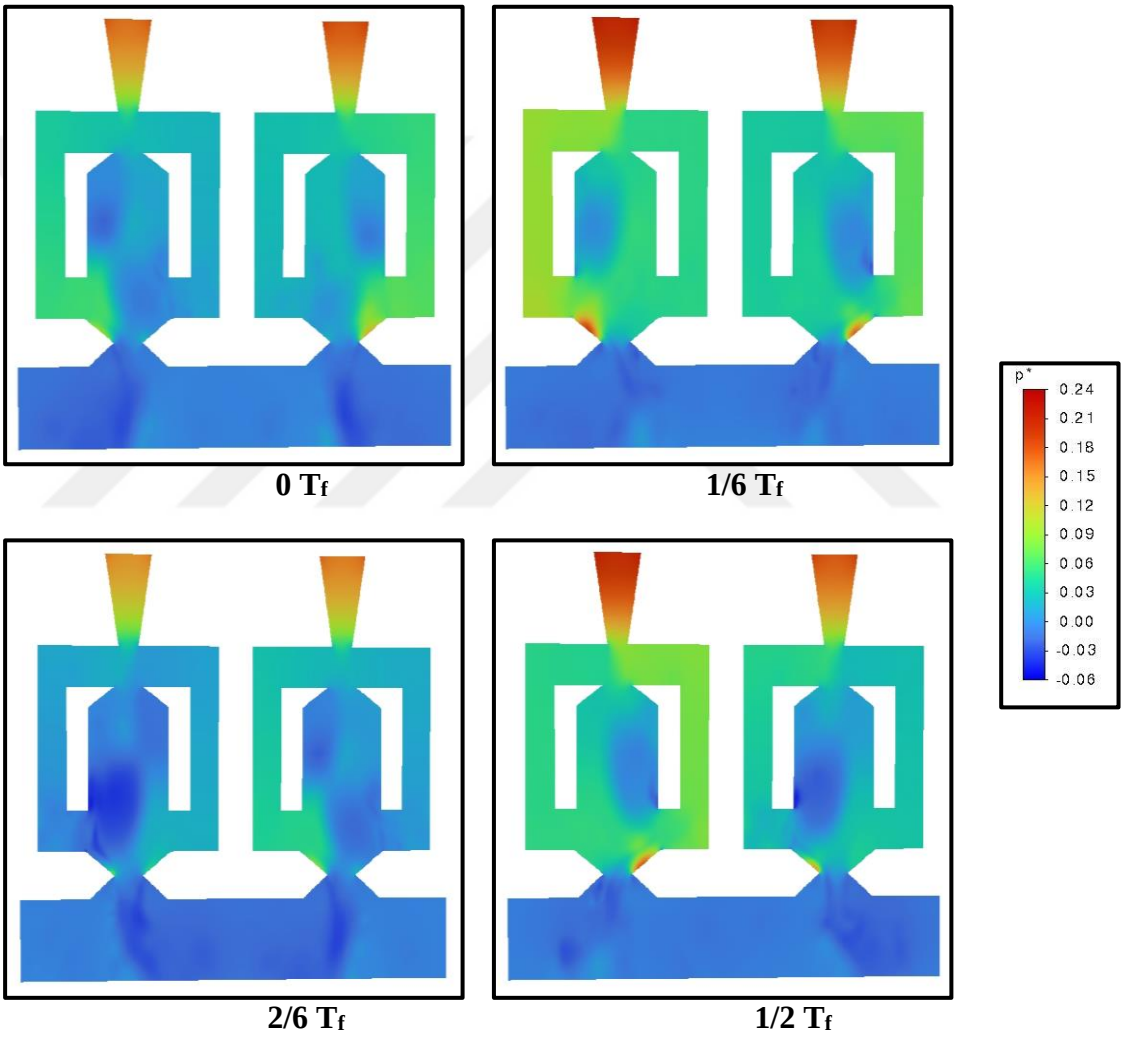

Figure 3.4 The Dimensionless Pressure Contour for Half Period at Re=3000

As the pressure in the channel increases due to the viscosity increase at the inlet of the fluidic oscillator, several changes may occur. An increase in the pressure typically results in an increase in fluid rate, fluid velocity, and fluid density. The pressure difference

between the inlet and outlet of the fluidic oscillator determines the fluid flow rate, while the pressure of the fluid at the inlet of the oscillator determines the fluid velocity. Furthermore, the pressure of the fluid in the channel affects its density. Additionally, an increase in pressure may cause a change in the amplitude of oscillation of the fluidic oscillator.

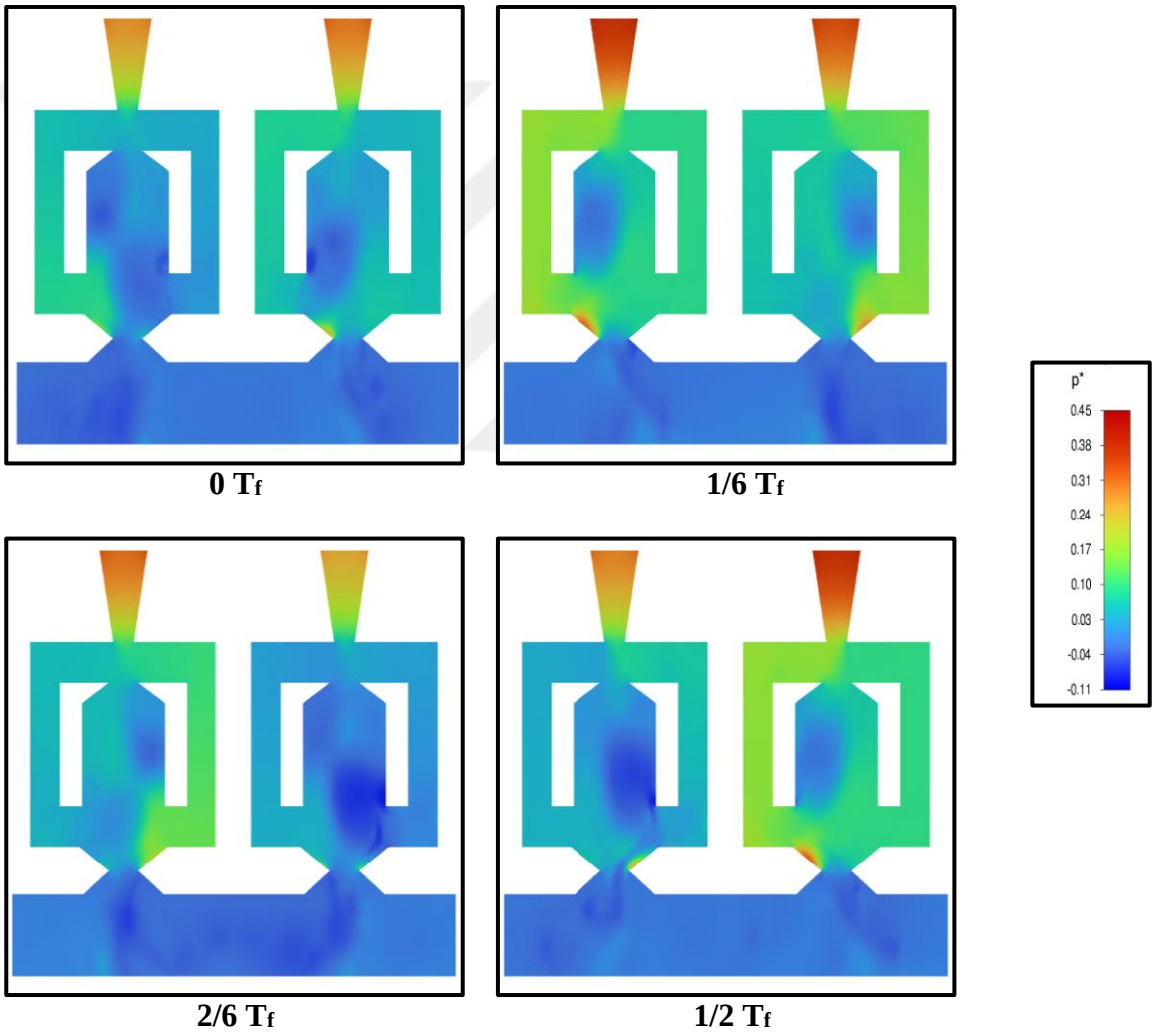

Figure 3.5 The Dimensionless Pressure Contour for Half Period at Re=4000

An increase in the coolant's pressure difference can enhance the heat transfer process in a heat exchanger. This is because a higher-pressure difference creates a stronger driving force for heat transfer and also increases the inlet flow rate, resulting in faster heat transfer.

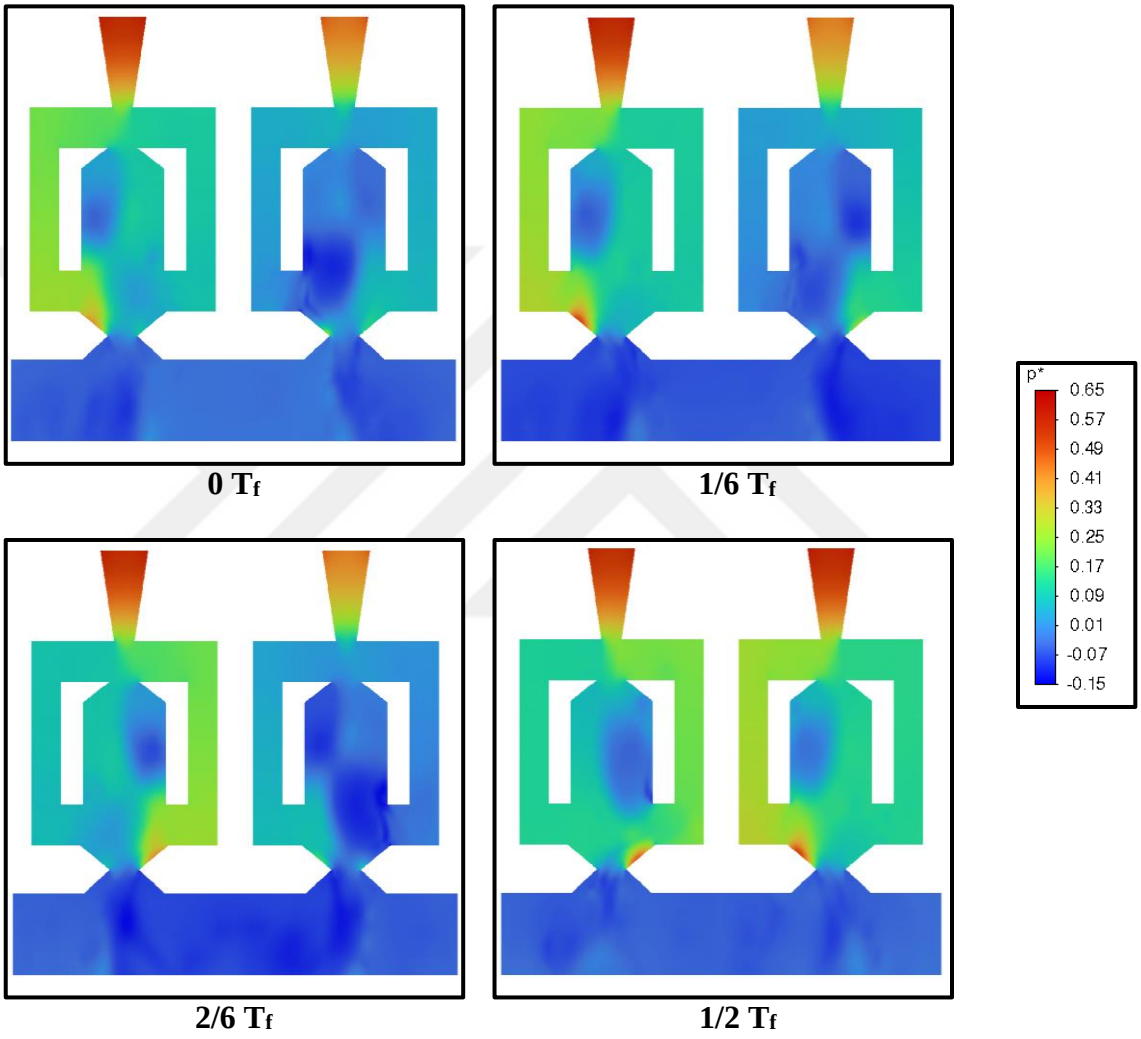

Figure 3.6 The Dimensionless Pressure Contour for Half Period at Re=5000

To investigate the impact of pressure difference on heat transfer, the system was evaluated at three different Re Numbers. The results indicate that the pressure difference increased as expected, which is consistent with the reference study. The observed increase in pressure difference can be seen in Figure 3.7, which displays the pressure difference values in units. The observed increase in pressure difference confirms the influence of

pressure difference on heat transfer, suggesting that it is a vital factor to consider when designing and optimizing heat exchangers.

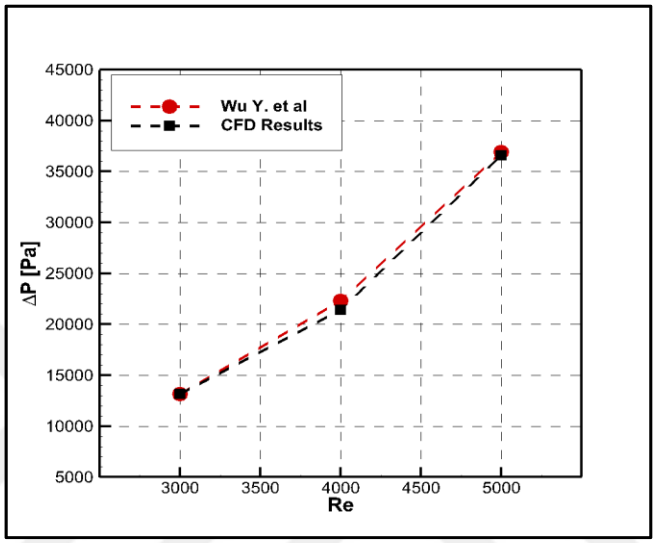

Figure 3.7 The Pressure Difference of the Flow at Different Re Numbers

3.2 Heat Transfer Result

To validate the CFD model, the results of the CFD analysis were compared with those of the reference study, which displayed similar characteristics. It has been established that oscillating flow can create turbulence, which leads to significant fluctuations, in the flow and a reduction in boundary layer thickness. In the reference study, the impingement surface, which has an area of LxW (9Dx15D), was investigated in terms of the time-averaged Nu number distribution on the impingement surface for X/L=0.25 and X/L=0.5.

The results, shown in Figure 3.8, indicate that the highest Nu value was found at the stagnation points, while there was a steep decrease in the Nu value at the center of the impingement surface. This is consistent with previous findings on impinging jets, where the maximum heat transfer rate occurs at the stagnation points due to the formation of a wall jet. The observed decrease in the Nu value at the center of the impingement surface

can be attributed to the boundary layer growth and flow separation caused by the interaction between the opposing jets.

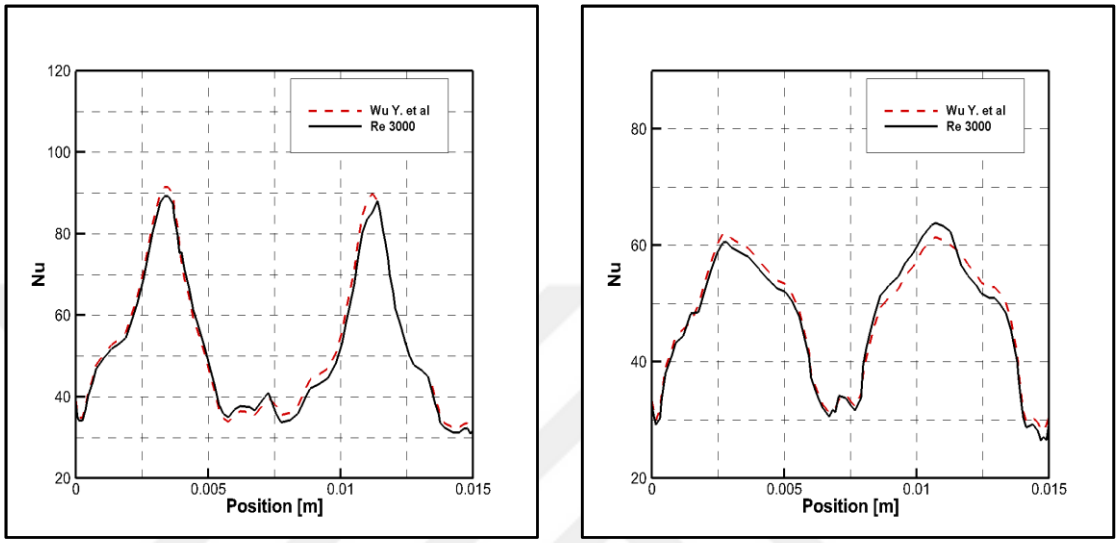

a) **b)**

Figure 3.8 The Time-averaged Distribution of the Nu Number for the **a)** X/L=0.25 and **b)** X/L=0.5 at Re=3000

When examining Figure 3.9 impingement jet flow at a Re number of 4000, it was observed that the maximum Nu number formed at the stagnation point increased as the fluid velocity increased, which is expected. Additionally, the minimum Nu number observed decreased. This behavior can be attributed to the increased turbulence and mixing of the fluid at higher velocities, resulting in enhanced heat transfer between fluid and the surface being cooled.

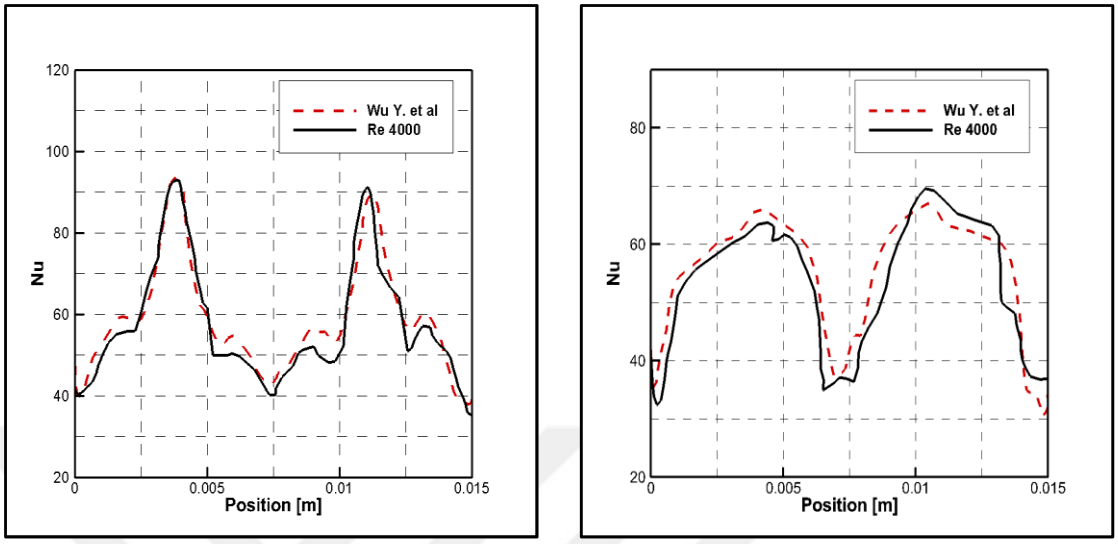

Figure 3.9 The Time-averaged Distribution of the Nu Number for the a) X/L=0.25 and b) X/L=0.5 at Re=4000

At a Re number of 5000, a similar behavior is observed in impingement jet flow, as depicted in Figure 3.10. The maximum Nu number formed at the stagnation point increases with increasing fluid velocity, while the minimum Nu number decreases. Additionally, the Nu number instantaneous decrease due to the wall jet effect occurs in a narrower range as the Re increases.

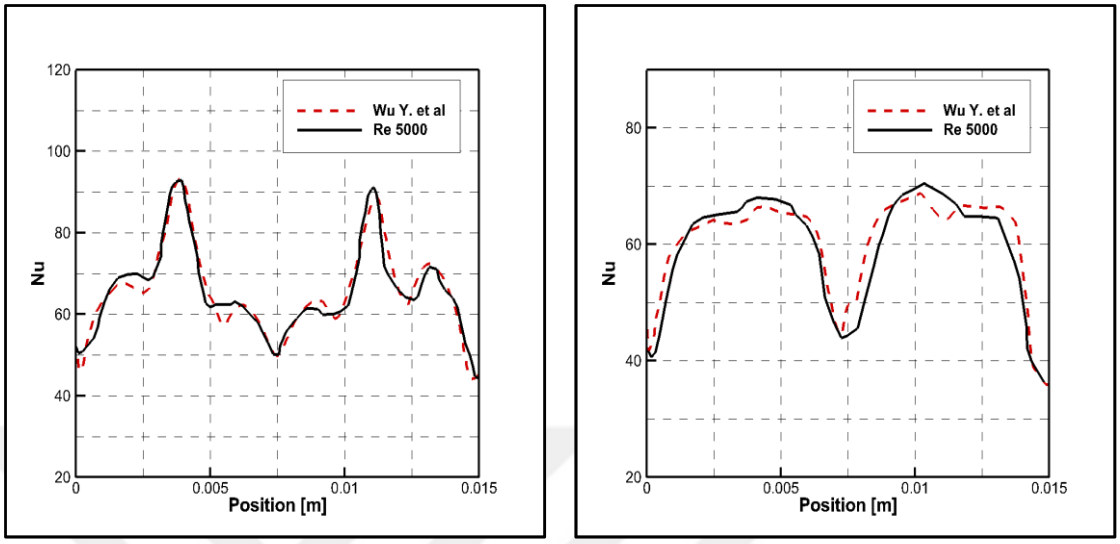

a) **b)**

Figure 3.10 The Time-averaged Distribution of the Nu Number for the a) X/L=0.25 and b) X/L=0.5 at Re=5000

In conclusion, the results suggest that the CFD model is reliable and that impingement surface characteristic should be considered when designing heat transfer systems, particularly in the case of impinging jets.

Upon examining the temperature values of the fluid in a channel, it was observed that the temperature values decreased as the Re number increased. This behavior can be attributed to the increased turbulence and mixing of the fluid at higher Re numbers, which can enhance the convective heat transfer from the fluid to the channel walls. Additionally, as the fluid velocity increases, the fluid spends less time in the channel, which can result in lower overall fluid temperatures.

It is important not, however, that the exact behavior of the fluid temperature in a channel is dependent on various factors such as fluid properties, channel geometry, and the type of heat transfer.

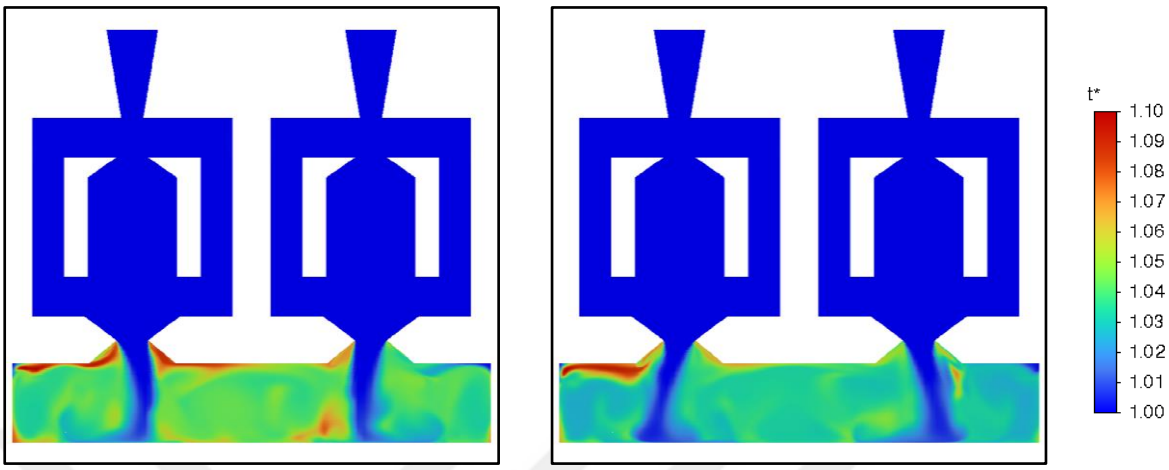

Figure 3.11 Non-dimensional Temperature Contour at Re=3000

During a validation study of fluid temperature behavior at different Re numbers, it was observed that the phenomenon of decreasing fluid temperature values with increasing Re number was consistent across all the Re numbers studied. Figure 3.11 depicts the dimensionless temperature value of the fluid over time, shown in the steps of 0 T_f to ½ T_f.

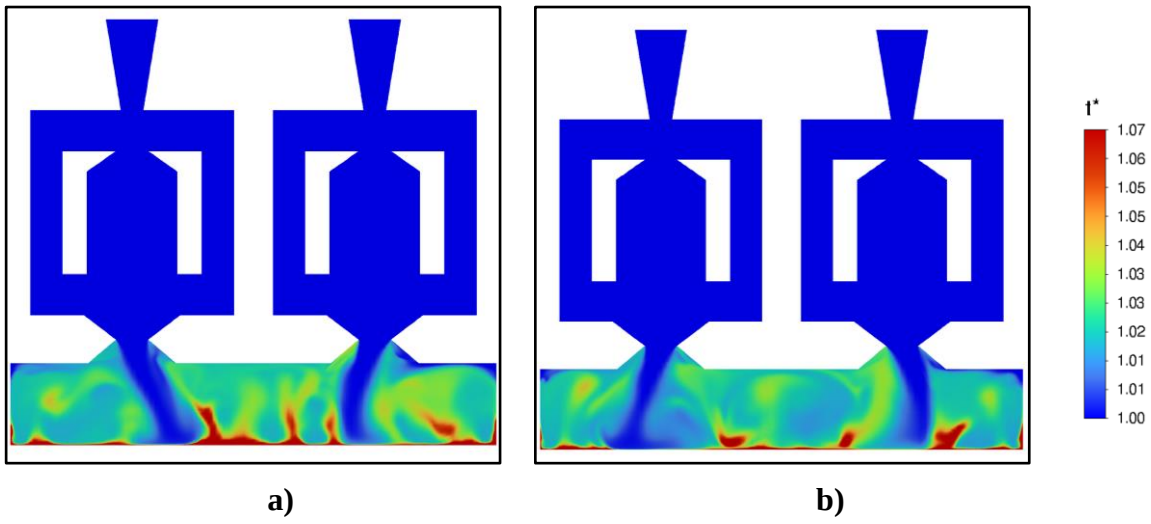

Figure 3.12 Non-dimensional Temperature Contour at Re=4000

As seen in Figure 3.12 and Figure 3.13 with an increase in Re number, the points where the maximum temperature appears decrease, while the turbulence of the flow increases. This can be attributed of the increased mixing and convective heat transfer caused by the higher turbulence intensity at higher Re numbers.

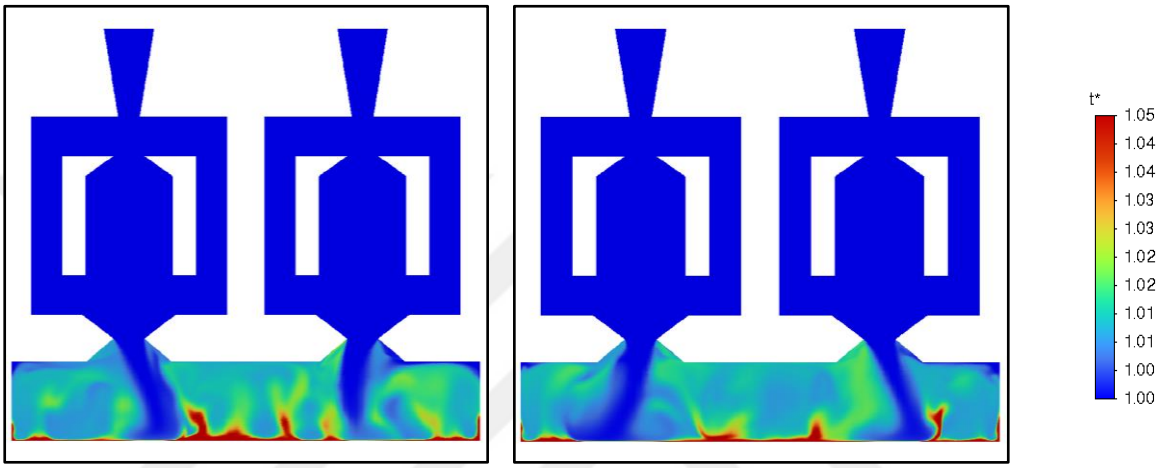

Figure 3.13 Non-dimensional Temperature Contour at Re=5000

There are several factors that affect the local Nu number on a surface, such as the physical properties of the fluid, the fluid velocity, the temperature difference between the fluid and the solid surface, the geometry of the solid surface, and the thermal conductivity of the solid surface. Additionally, the presence of obstructions in the flow, such as baffles or fins, can increase the heat transfer coefficient by promoting fluid mixing and improving surface area contact.

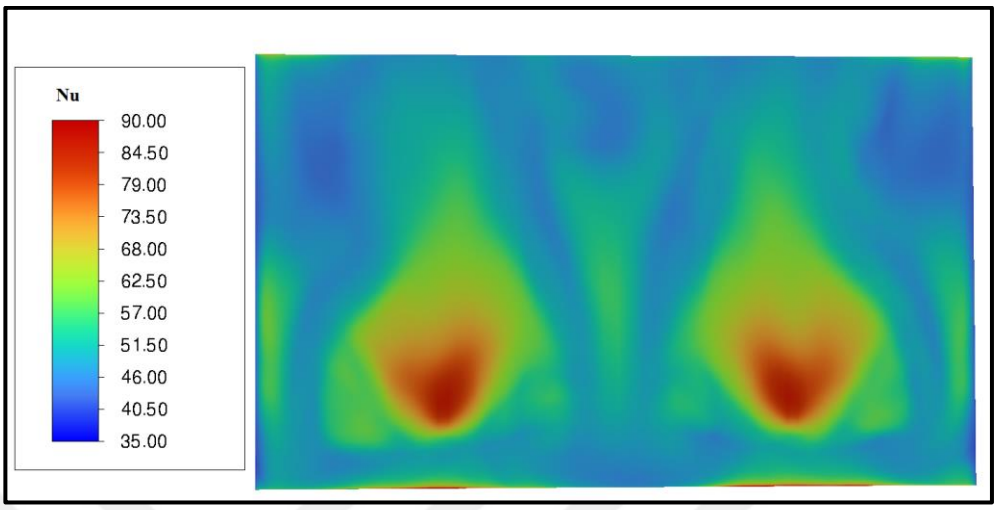

Figure 3.14 The Time-averaged Nu Number Distribution on Impact Surface at Re=3000

The furthermore, the Nu can be affected by the flow regime, such as laminar or turbulent flow, which can significantly affect the heat transfer coefficient. Therefore, an increase in the Re number will result in an increase in the maximum local Nu number. When examining the Figure 3.14 for Re 3000, it is observed that the maximum Nu number is 90, which occurs in the stagnation region. Since the flow oscillates, this stagnation zone spreads over a wide area.

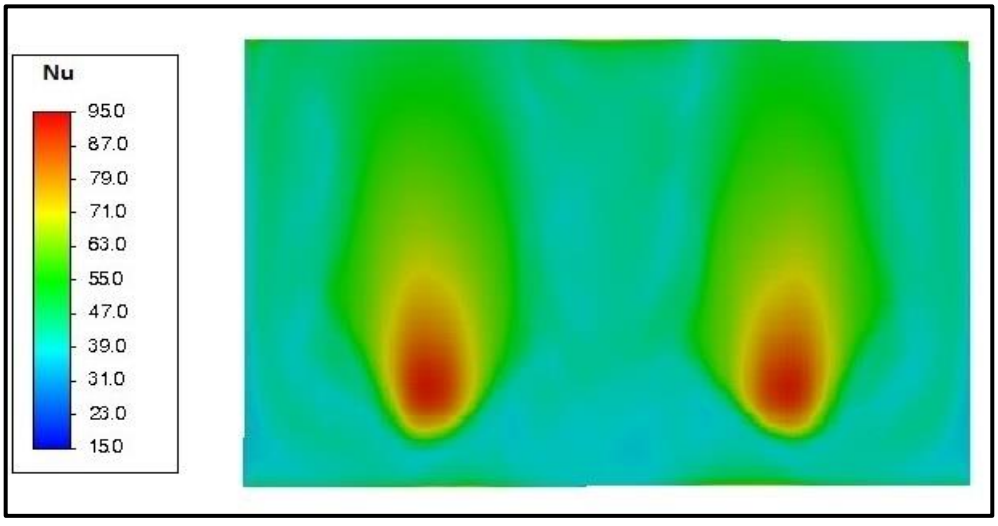

Figure 3.15 The Time-averaged Nu Number Distribution on Impact Surface at Re=4000

When the Figure 3.15 is examined for Re 4000, it is seen that the maximum values is the same, while the falling Nu value due to the jet wall effect is higher than that of 3000. This shows that the heat transfer performance increases due to the increase in flow oscillation. A similar situation applies to the Re 5000. When the Figure 3.16 is examined, it is seen that the values of the minimum Nu number on the impact wall increased compared to the other two results.

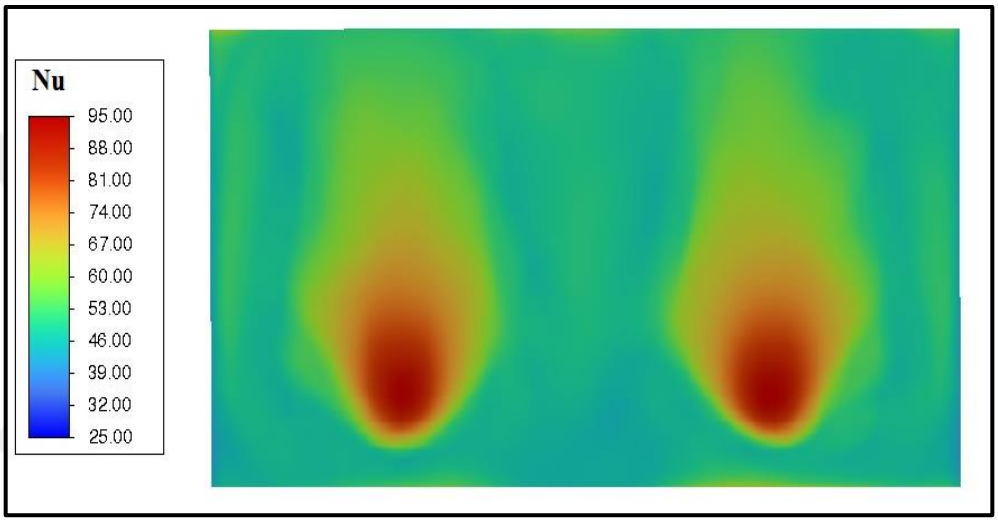

Figure 3.16 The Time-averaged Nu Number Distribution on Impact Surface at Re=3000

CHAPTER 4

RESULTS

After validating the CFD analysis method, the validated model was further analyzed by making some physical changes to investigate their effects on fluid dynamics and heat transfer. The aim of this investigation was to gain insights into the behavior of the fluid under different conditions and to optimize the design and performance of fluid oscillators in various applications.

Previous studies in the literature have investigated the effects of physical changes on fluid dynamics and heat transfer in fluidic oscillators. These physical changes include modifications to the dimensions of the chamber, the number and shape of the barriers, and the viscosity of the fluid. The effects of these changes have been analyzed through a series of simulations using validated CFD analysis methods.

Unlike previous studies, in this study, the effects of the impact angle of the jet fluid and the distance between the exit centers of the oscillator on fluid dynamics and heat transfer in fluid oscillators were investigated under two different headings. In the results section, the oscillation effect is shown in two time periods. These are the start time and the half time of oscillation.

4.1. Effect of Impact Angle

In this study, the impact angles of 30°, 45° and 60° are investigated, with Re values of 4000, 7000, and 10000 at each angle. The obtained results are examined in terms of internal fluid dynamics and heat transfer. The internal fluid dynamics results included the examination of the flow pattern, velocity distribution, and pressure drop. Heat transfer results included the study of the temperature distribution and Nu number distribution. The following sections will present the findings and discussions of these analyses.

4.1.1. Internal Fluid Dynamic Result

Internal fluid dynamics play a crucial role in numerous engineering applications, including heat exchangers, pumps and turbines. Understanding the behavior of fluids inside these systems is essential for optimizing their performance and improving their efficiency. CFD is a widely used tool for studying internal fluid dynamics, allowing for detailed simulations of fluid flow and heat transfer. In this study, it is explored the internal fluid dynamic results of a microchannel heat exchanger using two fluidic oscillators to enhance the heat transfer performance in impinging jet cooling.

The aim of this research is to gain insight into the flow behavior and heat transfer characteristics of the fluid inside the microchannel heat exchanger and to provide useful data for the optimization of such systems. To comprehend both the oscillation and the bubble forms generated during the oscillation, it is customary to display the results on the X=0 plane.

4.1.1.1. Angle of 30°

The analysis of the results for Re 7000 and 10000 will be presented in this section. However, it is important to note that the results obtained for Re 4000 is discussed separately under the title of validation study.

At a Re Number of 7000, the interaction between the incoming flows and the main jet inlet region causes a deflection of the jet due to the pressure difference in the two feedback channels, as demonstrated in Figure 4.1. During half of the oscillation period, the fluid adheres to the right wall of the nozzle of the first oscillator and the left wall of the nozzle of the second oscillator. A portion of the fluid was also flows towards the feedback channel and returns to the inlet of the oscillator. The formation of a bubble in the mixing region pushes the incoming fluid, causing it to adhere to the opposite wall. In the subsequent time step, the bubble disappears as it enters the feedback channel and exits through the outlet. This process is repeated on the opposite wall, resulting in self-sustaining sweeping.

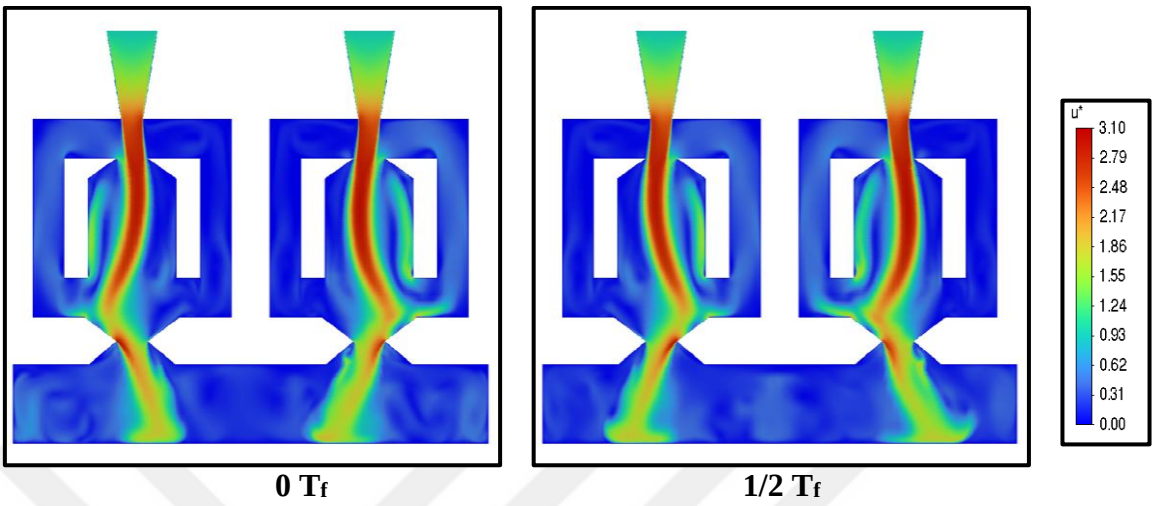

Figure 4.1 The Dimensionless Velocity Contour for Half Period at Re=7000

It was observed that the heat transfer started to increase with the increase of the impact surface with the increase of the impact surface with the change of the velocity, frequency and amplitude of the fluid to the impact surface. This whole process takes place after the oscillation starts, regardless of the Re value. However, as the Re value increases, the pressure difference in the channel increases. Figure 4.2 shows the dimensionless pressure distribution which also indicates a similar process. As the jet stream sticks to the right wall of the nozzle, it generates high pressure in the left feedback channel, while negative pressure is observed on the right side of the mixing chamber due to the formation of a bubble.

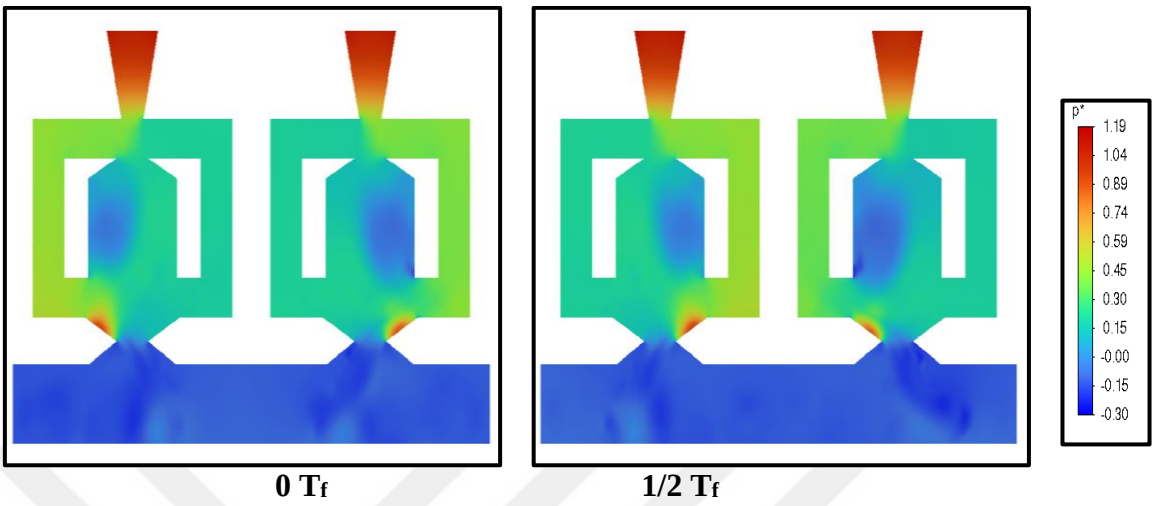

Figure 4.2 The Dimensionless Pressure Contour for Half Period at Re=7000

With the increase of Re number (Figure 4.3) at the inlet of the fluidic oscillator, the velocity profile has become more complex due to the occurrence of various flow phenomena such as turbulence and eddies. The flow becomes more chaotic and unstable, resulting in larger bubbles and an increase in the phase angle of the jet stream, as well as a larger area of action.

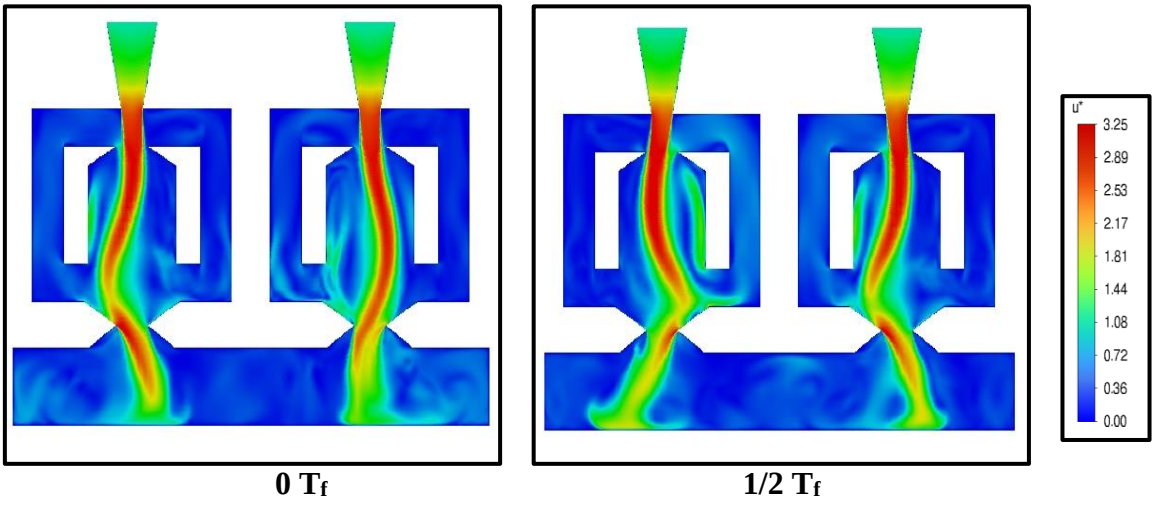

Figure 4.3 The Dimensionless Velocity Contour for Half Period at Re=10000

As seen in in Figure 4.4, the pressure value in the channel has increased. The highest pressure was observed at the inlet, where the fluid adhered to the nozzle wall. Conversely the lowest pressure was recorded in the area where the bubbles was formed, resulting in a vacuum effect that facilitated fluid flow.

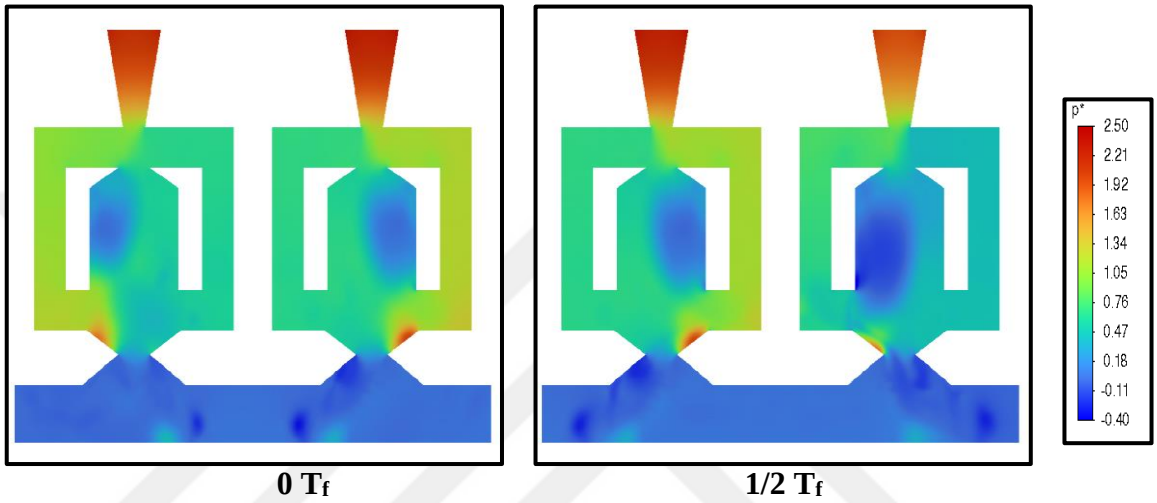

Figure 4.4 The Dimensionless Pressure Contour for Half Period at Re=10000

4.1.1.2. Angle of 45°

The impact angle of the coolant on the surface has a significant effect on pressure drop measurements, owing to the larger area over which the fluid is spread, thereby changing the surface roughness and causing a variation in the direction of traction. However, the relationship between impingement angle and pressure drop may not be linear and may vary based on the specific measurement. The study investigated the effect of impingement angle on pressure drop measurements by increasing the angle of impact from 30° to 45°. The findings showed an increase in the pressure difference between the inlet and channel outlet as the angle of impact increased. The results of the analysis showed that the pressure difference between the inlet and channel outlet increased as the angle of impact increased, and this trend remained unchanged when the Re number was varied.

To compare the intra-channel velocity variation, it would be appropriate to examine the dimensionless velocity values at the same Re number for the 30° impact angle. When the impact angle is 30°, the maximum velocity for the Re number for 4000 is 3.10, while it is seen from Figure 4.5 as 3.20 when the impact angle is 45°.

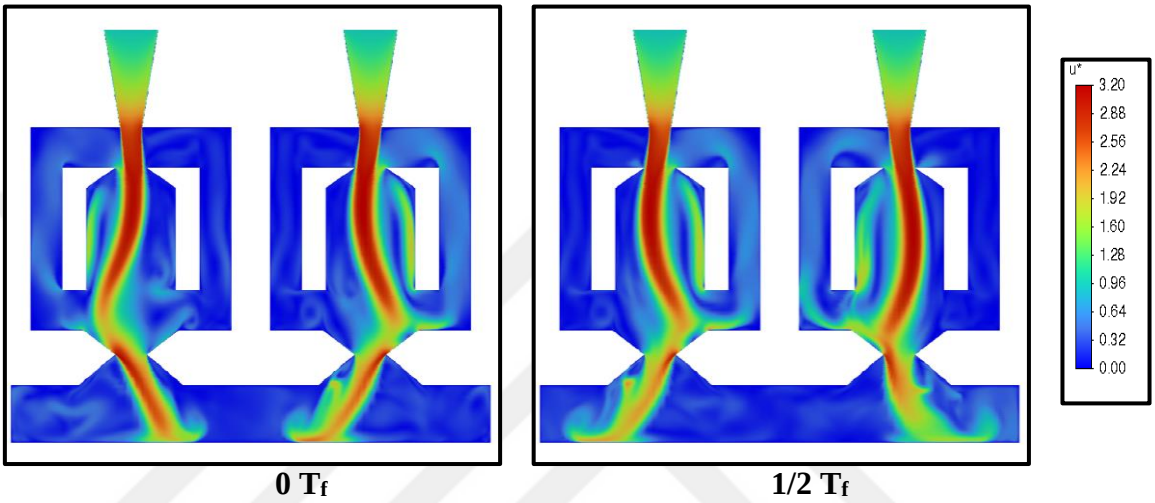

Figure 4.5 The Dimensionless Velocity Contour for Half Period for 45° at Re=4000

An increase in the flow rate in the channel results in a higher flow rate, which indicates an increase in the pressure difference between the inlet and outlet of the channel. When examining the dimensionless pressure distribution of the channel, it was observed that at a Re number for 4000, the maximum pressure was 0.45 for an impact angle of 30° and 0.48 for an impact angle of 45°. (from Figure 4.6) This indicates an approximately 9% increase in pressure difference with the increase in the angle. When the pressure difference increases, the fluid flow rate in the channel also increases. This increased velocity causes the bubble to stretch and deform, resulting in an elongated and smaller diameter separation bubble. The lower pressure of the liquid in this region, which is typically lower than the operating pressure, leads to the creation of negative pressure or suction. In addition, the increased pressure difference may cause the separation bubble to move more rapidly along the channel, resulting in changes in the bubble's behavior, such as increased frequency of bubble formation or bursting.

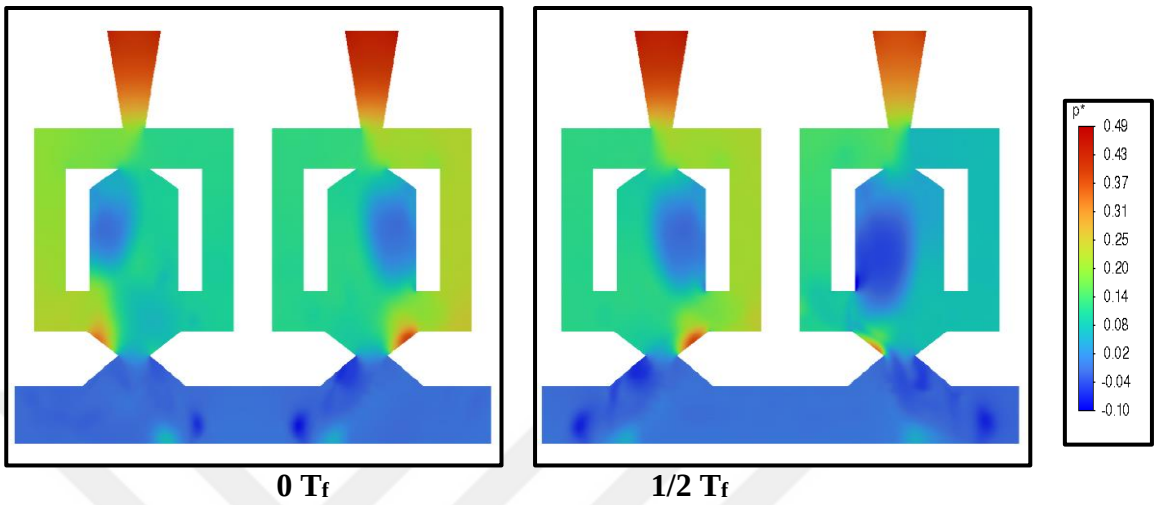

Figure 4.6 The Dimensionless Pressure Contour for Half Period for 45° at Re=4000

As part of the validation study, it was observed that the internal flow and heat transfer performance increased as the Re number increased. In this context, the results of the highest Re value were examined.

When the velocities in the channel were examined at Re 10000, it was found that the greatest dimensionless velocity was 3.40. (from Figure 4.7) This result was contrasted with the earlier recorded value of 3.25, which was made for the identical Re Number and impact angle of 30°. The maximum velocity within the channel increases as the impact angle increases, it can be deduced.

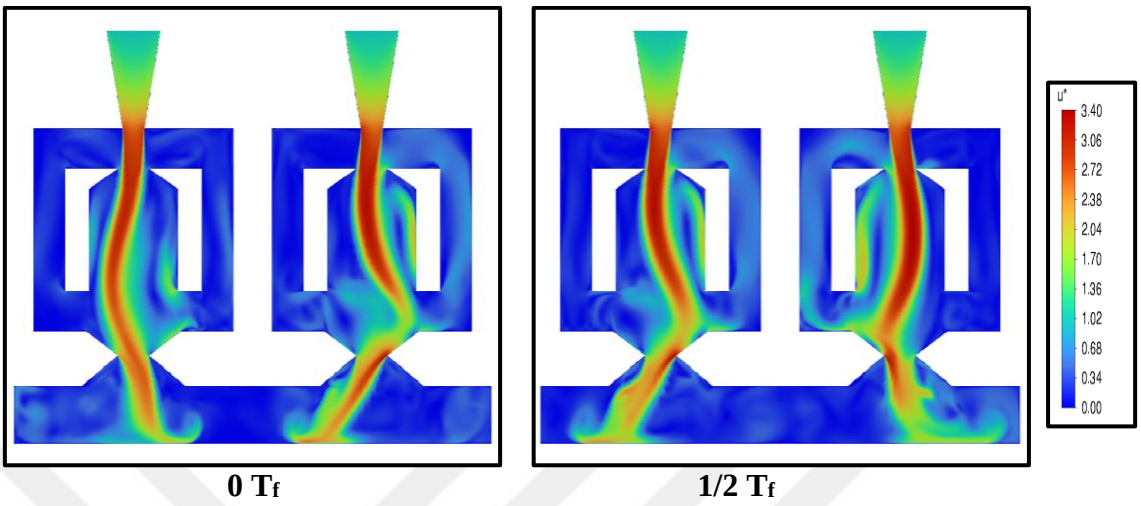

Figure 4.7 The Dimensionless Velocity Contour for Half Period for 45° at Re=10000

The pressure difference in the duct and, consequently, the maximum pressure to be created will both grow as the Re value and impact angle increase. The maximum dimensionless pressure value was found to be 2.80 when the Figure 4.8 was inspected. The maximum pressure increased by 12% when the model was analyzed with an impact angle of 30°.

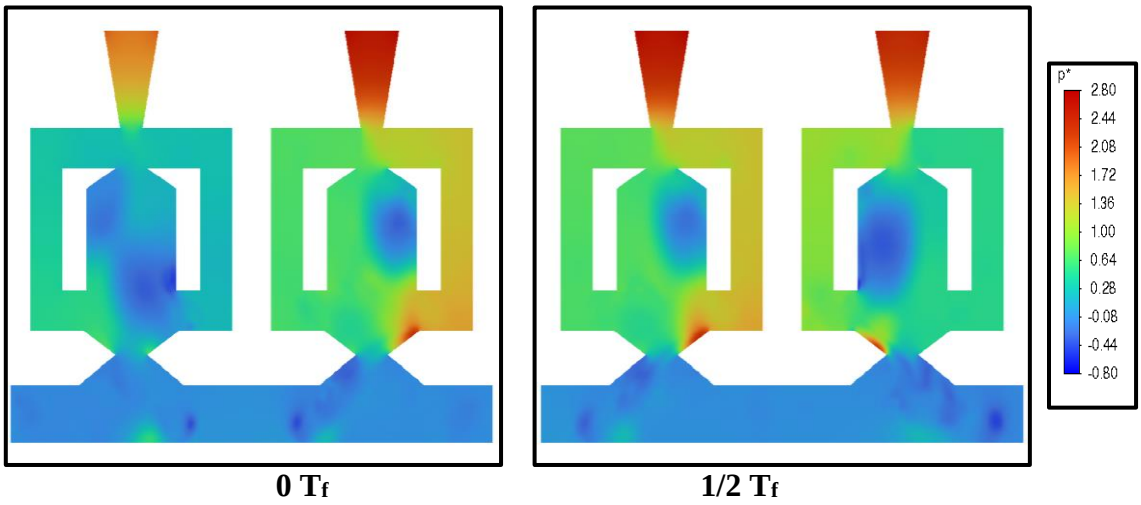

Figure 4.8 The Dimensionless Pressure Contour for Half Period for 45° at Re=10000

4.1.1.3. Angle of 60°

To investigate the effects of changing the impact angle, a model with an impact angle of 60° was analyzed at three different Re numbers. The results for Re numbers of 4000 and 10000 will be presented to assess the impact angle of the angle and the Re number on the physical phenomena observed.

The maximum velocity increases noticeably when compared to the other two angles, and the oscillation occurs over a wider frequency range, as can be seen in Figure 4.9 when the velocity contours in the channel for Re 4000 are inspected.

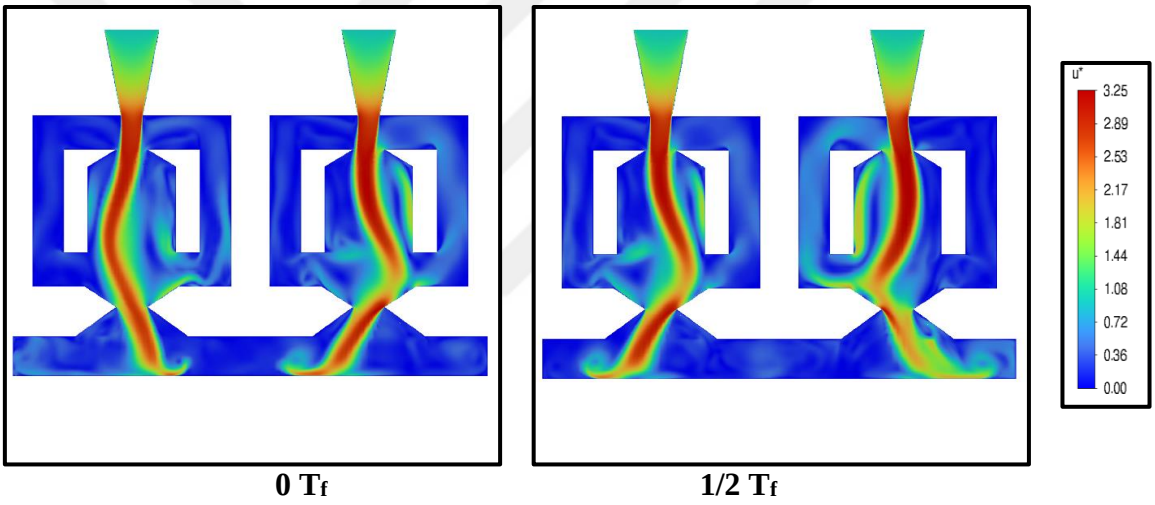

Figure 4.9 The Dimensionless Velocity Contour for Half Period for 60° at Re=4000

The size and shape of the vortices that form in the mixing chamber fluctuate along with the impingement angle, which alters the pressure distribution in the fluidic oscillator. The size and length of the eddies generated increased with the contact angle. As a result, the low-pressure area becomes more pronounced while the high-pressure area movers further downstream.

When inspecting the Figure 4.10, it can be observed that both the pressure difference in the duct and the maximum pressure created increase as the Re value and impact angle

increase. The maximum dimensionless pressure value, which was found to be 0.56, also supports this observation.

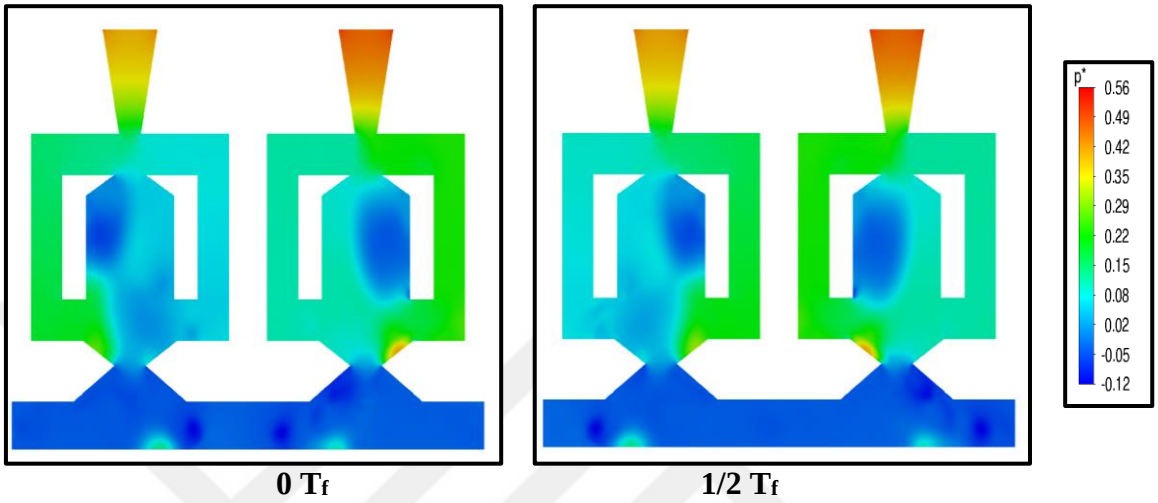

Figure 4.10 The Dimensionless Pressure Contour for Half Period for 60° at Re=4000

The results indicated that as the angle of impact increased, so did the pressure difference between the channel's intake and outflow. The analysis's findings demonstrated that as the angle of impact grew, the pressure difference between the inlet and channel exit increased.

This trend persisted even when the Re number was modified. It would be helpful to look at the dimensionless velocity readings at the same Re number for the 30° and 45° impact angles in order to compare the intra-channel velocity variance. The maximum velocity for the Re number for 10000 at impact angles of 30° and 45° is 3.25 and 3.40 but for impact angle of 60° is 3.50, respectively. (from Figure 4.11)

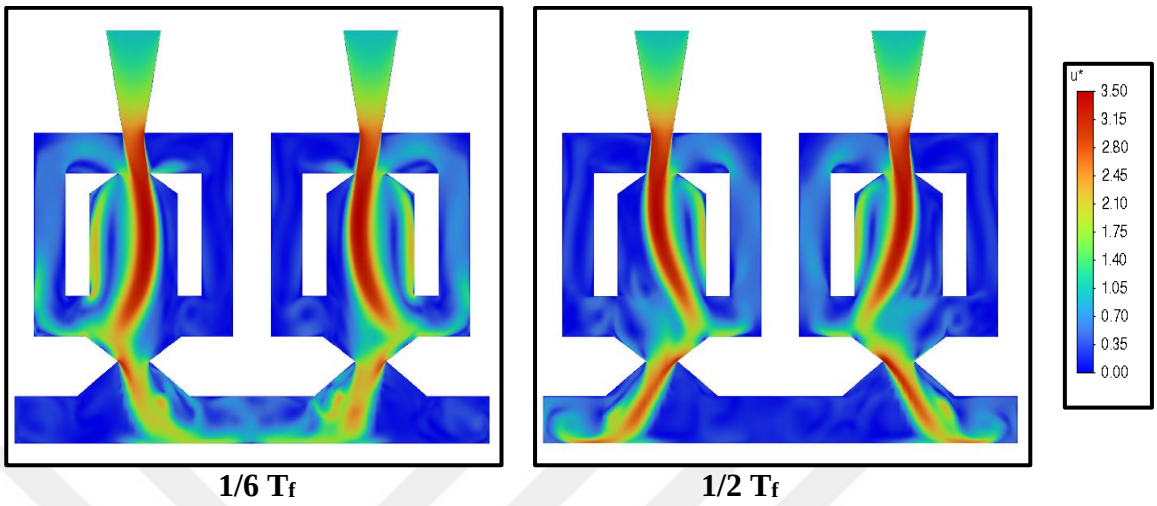

Figure 4.11 The Dimensionless Velocity Contour for Half Period for 60° at Re=10000

It is possible that when the fluid flows through the channel and contacts the geometric characteristics, low pressure zones occur, explaining why the lowest pressure may be seen in the area where the bubbles form when the figure is studied. The development of bubbles may also help to lower the pressure in this region, creating a vacuum effect that makes it easier for fluid to flow.

The model and Re number with the highest dimensionless pressure value among all shared findings is represented by the Figure 4.12. It is crucial to keep in mind that the pressure distribution in a fluidic oscillator can be intricate and reliant on a number of elements, such as channel's geometry and the frequency and amplitude of the oscillations.

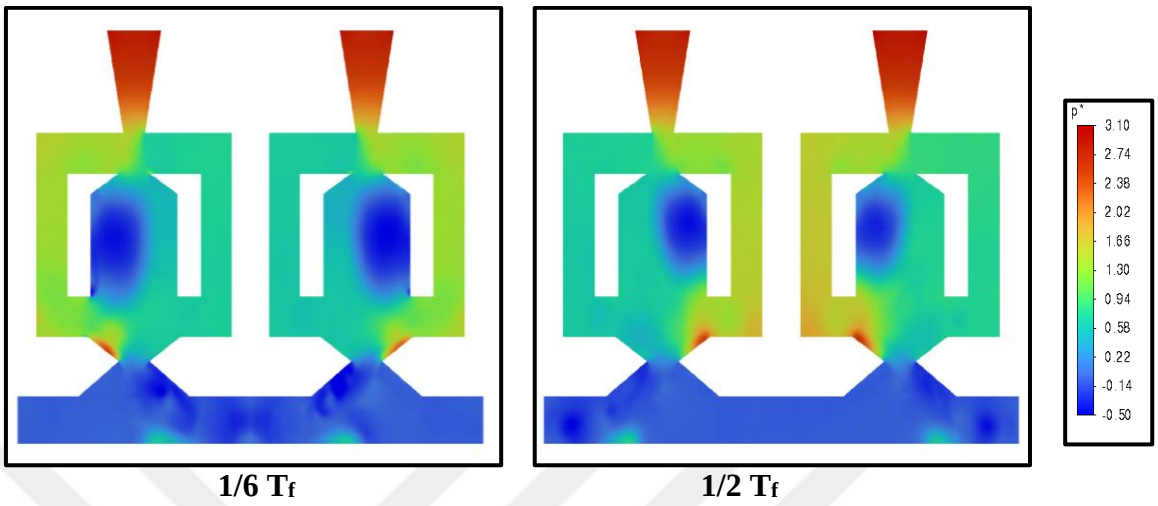

Figure 4.12 The Dimensionless Pressure Contour for Half Period for 60° at Re=10000

For various Reynolds numbers and impact angles of 30°, 45°, and 60° degrees, the Figure 4.13 displays the mean dimensionless pressure values. The findings show that as the impact angle increases, so does the mean dimensionless pressure value. Higher pressure levels are the result of an increase in fluid momentum and kinetic energy in the direction perpendicular to the surface.

Furthermore, even at low Reynolds numbers, it is seen that the difference between the mean dimensionless pressure values grows as the Reynolds number rises. This is explained by the fact that with higher Reynolds numbers, the turbulence severity and flow complexity increase, leading to larger pressure fluctuations.

The impact angle of 60° and the Re number of 10000 produce the highest average pressure value, which is 2.2. This finding suggests that the impact angle has a greater influence on the pressure distribution on the surface at higher Re numbers. This result is in line with the literature, which shows that the Re number and impact angle among other flow parameters have an impact on the pressure distribution on a surface subjected to fluid flow.

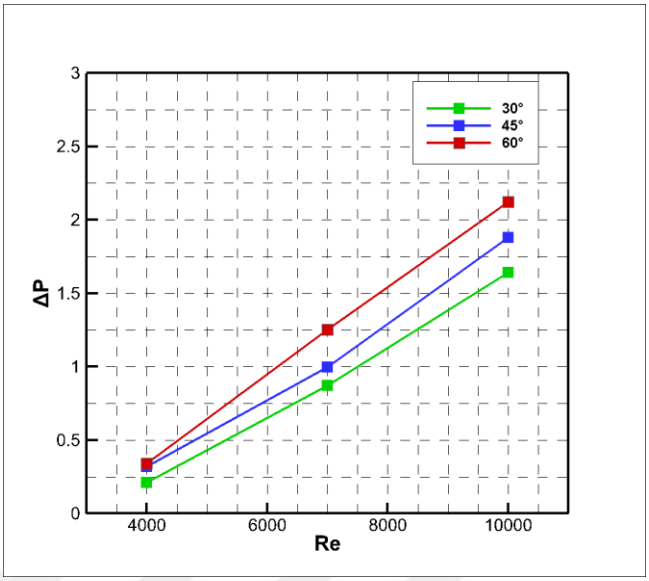

Figure 4.13 The Dimensionless Pressure Drop of the Flow at Different Impinging angle with respect to Various Re Numbers

4.1.2. Heat Transfer Result

It has been discovered that oscillating flow can produce turbulence, which can cause considerable flow variations and a drop in the thickness of the boundary layer. When model validation analyses were performed, the CFD analysis results showed a similar feature to the reference work.

Additionally, it was discovered through the internal flow analysis that as the impact angle and Re number value increased, so did the pressure difference in the channel, and as a result, the flow's frequency and velocity. On heat transfer, a similar phenomenon is anticipated. The results will be demonstrated in this section by comparison with various scenarios since the results are detailed in the internal fluid dynamics section.

The time-averaged Nu number on the surface exhibits distinct fluctuations in the two result in Figure 4.14, which represent the impact of a fluid on a surface at various angles of 30° and 60°, respectively. The value of the time-averaged Nu number increases from 30° to 60° of impact angle, showing an increase in convective heat transfer coefficient.

This is explained by an increase in the fluid's component of velocity perpendicular to the surface, which speeds up heat transfer.

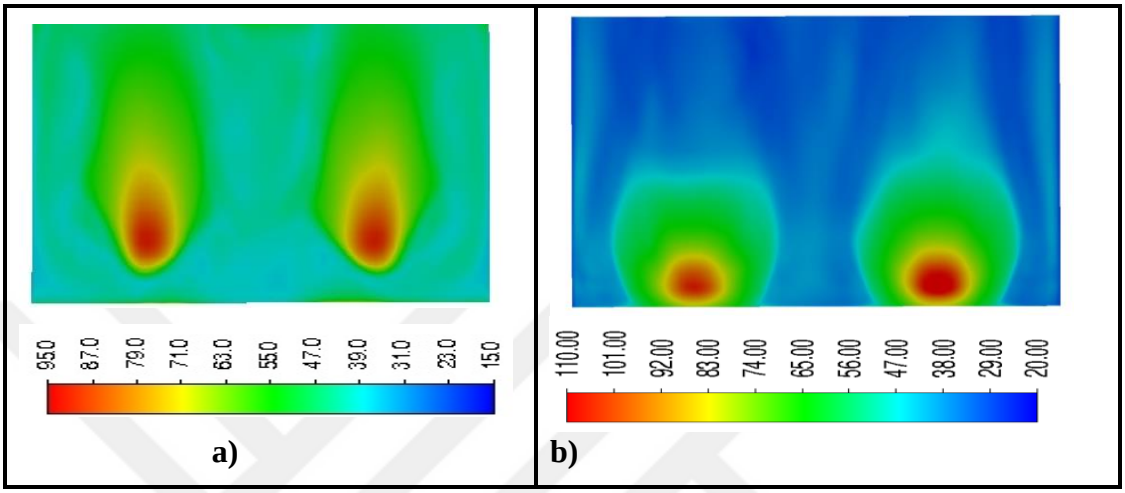

Figure 4.14 The Time-averaged Nu Number Distribution on Impact Surface at Re=4000 for a) Angle 30° and b) Angle 60°

Additionally, the maximum Nu number on the surface is affected by the change in impact angle. The greatest Nu number shifts toward the leading edge of the surface as the angle of impact increases, suggesting a faster rate of heat transfer there. This change can be attributed to the fluid at the leading edge exerting more shear stress due to the larger impact velocity component parallel to the surface.

The time-averaged Nu number on the surface is presented in Figure 4.15 along with two result images illustrating the impact angle's impact on heat transmission at various angles of 45° and 60°. The value of the time-averaged Nu number rises as the impact angle rises from 45° to 60°, demonstrating an increase in the convective heat transfer coefficient. This is in line with the findings in the internal fluid dynamics section's conclusion paragraph, which demonstrate that as the fluid's impingement angle increases, so does the flow velocity and, thus, the heat transfer coefficient.

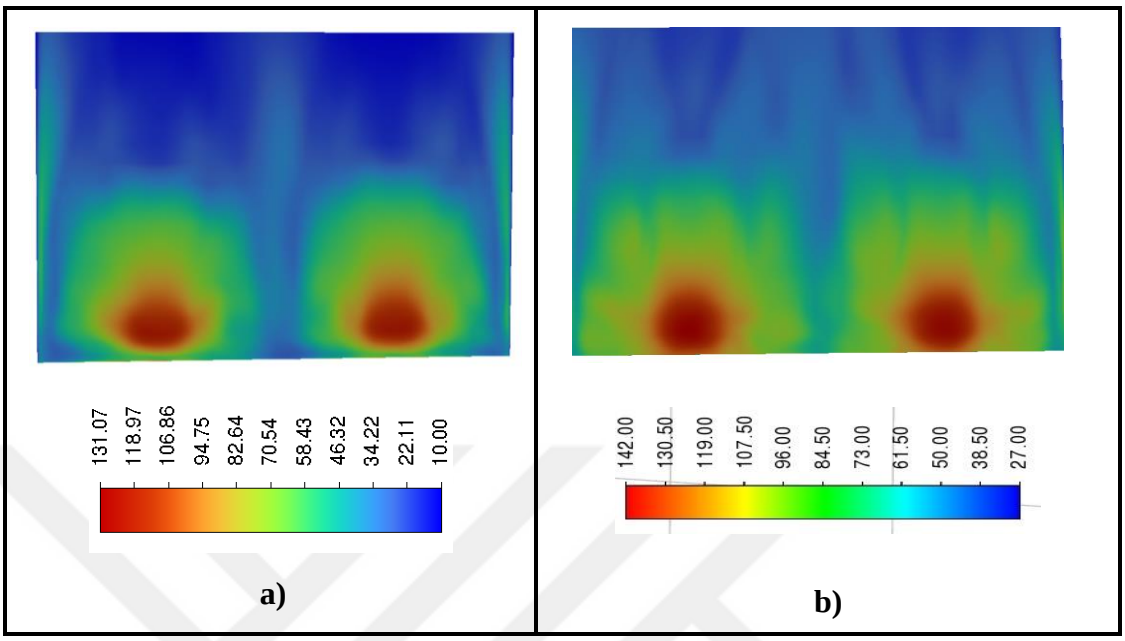

Figure 4.15 The Time-averaged Nu Number Distribution on Impact Surface at Re=7000 for a) Angle 45° and b) Angle 60°

The position of the greatest Nu number on the surface is likewise impacted by changes in the impact angle. The maximum Nu number in this instance shifts toward the leading edge of the surface as the impact angle rises.

This is because the fluid near the leading edge exerts more shear stress, which increases the rate of convective heat transfer in that area. The impact angle of 60° has a larger maximum Nu value than the impact angle of 45°, indicating a higher rate of convective heat transfer for the former. This result is in line with the literature, which claims that as the fluid's impact angle increases, so does the heat transfer coefficient. It's possible that the unique conditions and model parameters are the reason for the relatively minor variation between the maximum Nu values for the two impact angles.

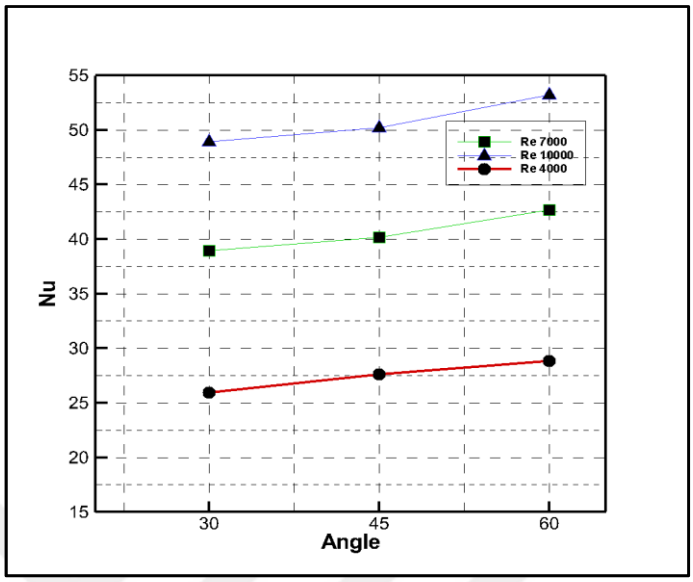

Figure 4.16 The Time-averaged and Area-averaged Nu Number Value

The average Nusselt numbers for various Re numbers and impact angles of 30°, 45°, and 60° are shown in Figure 4.16. According to the findings, the average Nusselt number rises as the Re number and impact angle rise. The literature, which states that an increase in Re number results in improved convective heat transfer due to higher turbulence intensity and flow complexity, is consistent with this pattern. Additionally, the fluid's increased impact angle causes it to exert more shear stress on the surface, which raises the convective heat transfer coefficient. As a result, as the impact angle increases, so does the average Nu number value on the surface.

The impact angle of 60° with the Re number of 10000 provide the highest average Nu number value, which is 53. This result demonstrates that the convective heat transfer coefficient increases noticeably when the fluid's impingement angle increases at higher Reynolds numbers. The increase in frequency is what causes the heat transmission to improve as the Re number rises. Although the frequency increase is inversely proportional to Re number, studies conducted in the literature have shown that it is constant after a certain value. Therefore, it should be remembered that the improvement in heat transfer will increase as Re number is raised.

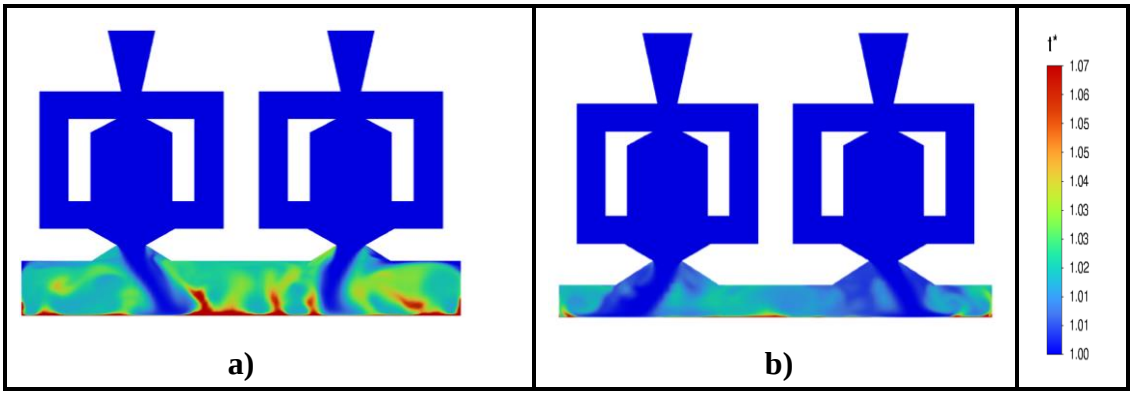

Figure 4.17 Non-dimensional Temperature Distribution at Re=10000 for a) Angle 30 and b) Angle 60

In order to more clearly see how the severity of the turbulence changes, a common scale is utilized in the offered Figure 4.17 to depict the dimensionless temperature contour for various impact angles. The findings show that the impacts of the sweep in the jet flow and the ensuing flow variations increase with increasing impact angle. This observation is in line with the literature, which claims that an increase in impact angle causes an increase in the complexity of the flow and the intensity of the turbulence. The contour also demonstrates that when the impact angle increases, the dimensionless temperature in the channel falls. This phenomena can be explained by the fact that as the velocity component parallel to the surface rises, the convective heat transfer coefficient may also rise.

A lower dimensionless temperature in the channel can be caused by this effect's shorter residence time since it can minimize the amount of heat transported to the surface. It is crucial to keep in mind, though, that the impact angle can also have an impact on the flow's level of turbulence, how the heat flux is distributed on the surface, and the convective heat transfer coefficient.

4.2. Effect of Distance Between Oscillator Outlet Centers

Fluid oscillators' performance is significantly influenced by geometrical factors, such as the separation between their centers. Finally, this study looked into how fluid oscillator array performance was affected by center-to-center distance. D is the diameter of the

oscillator orifice, and three distinct center-to-center distances, 7D, 7.5D, and 8D, were taken into consideration. The impact angle was held constant at 30° throughout the trials, which were run at three different Re values.

The findings for Re 7000 of models with 8D and 7D distances between centers are shown in Figure 4.18 and Figure 4.19, respectively. When the results were examined, it was found that as the distance between the centers got smaller, the maximum dimensionless pressure value in the channel increased and the pressure difference did as well.

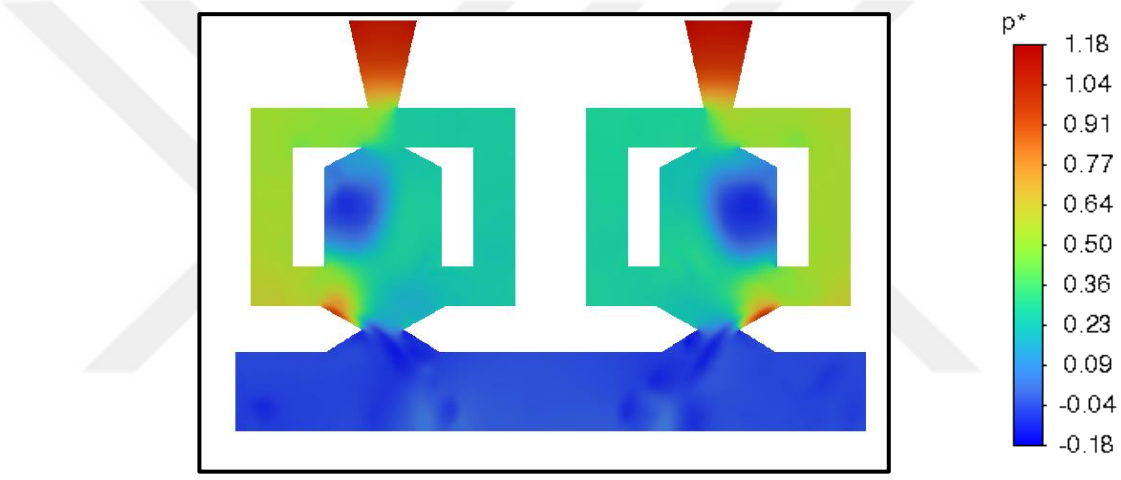

Figure 4.18 The Dimensionless Pressure Contour 1/2Tf for 8D at Re=7000

The highest dimensionless pressure was 1.18 when the distance between the centers was 8D, whereas this number was determined to be 1.28 when it was 7D.

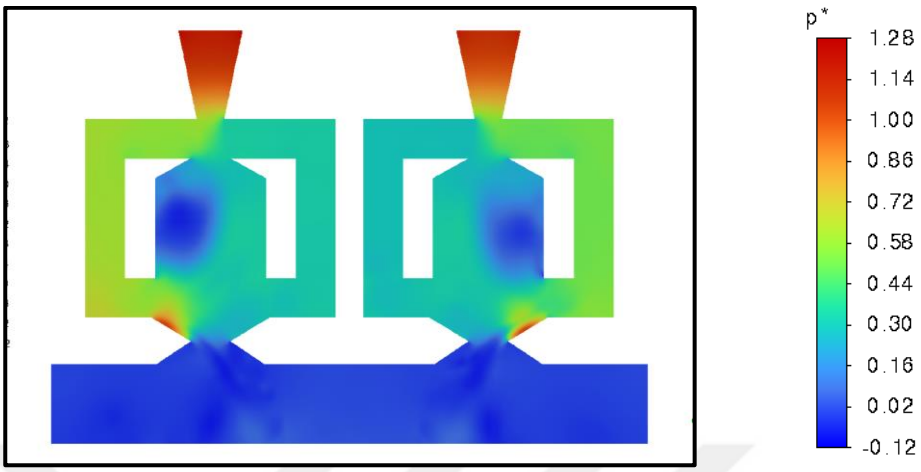

Figure 4.19 The Dimensionless Pressure Contour 1/2Tf for 7D at Re=7000

The development of a stronger and more coherent vortex structure in the flow can be used to explain why there is an increase in pressure difference in the channel as the distance between oscillator arrays decreases.

The vortices produced by each oscillator array are increasingly isolated and interact less vigorously as the distance between them increases. Since there is less mixing and heat transfer between the fluid and the surface, the flow field is characterized by weaker, more randomly distributed vortices.

On the other hand, when the distance between the oscillator arrays decreases, stronger interactions between the vortices produced by each array result in the production of bigger, more coherent vortices. As was indicated in the part before, a rise in pressure differential also causes an increase in duct velocity, which raises the convectional heat transfer coefficient. This case also involved a similar occurrence that was seen.

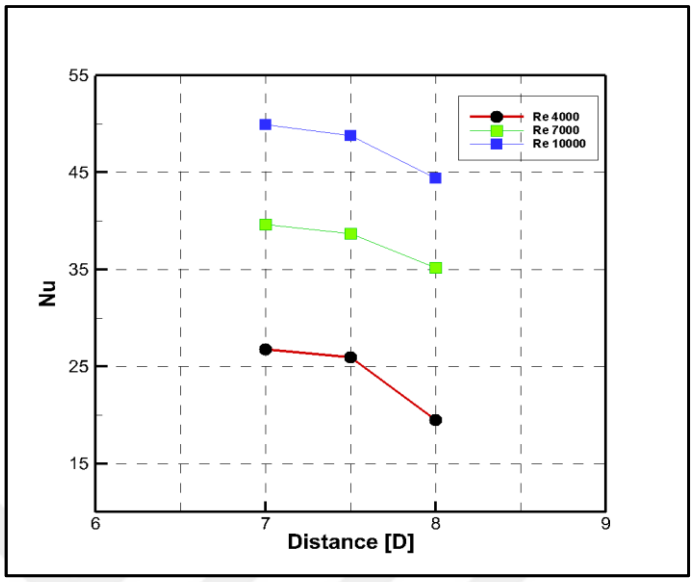

Figure 4.20 The Time-averaged and Area-averaged Nu Distribution for Various Distance

Examining Figure 4.20 reveals that the surface average Nu value rises as the space between the centers gets smaller. The heat transfer coefficient, which describes a fluid's capacity to transmit heat to or from a surface, and the surface average Nu value are connected. When an oscillator array's centers are closer together, the fluid near the surface oscillates more frequently, which can improve mixing and raise the heat transfer coefficient. This is so that the oscillatory motion can improve the transfer of heat from the surface to the fluid by dispersing the boundary layer close to the surface.

Additionally, a reduction in the distance between the oscillator array's center points may cause the development of vortices, which may improve fluid mixing and heat transfer. Better heat transfer from the surface to the fluid can result from the fluid mixing more thoroughly and from the vortices, which can also reduce the thickness of the boundary layer. Therefore, it's possible that the increased mixing and vortex formation that occurs as the distance between the oscillator array's centers decreases, which increases the surface average Nu value, is what causes the change in the heat transfer coefficient between the surface and the fluid. Additionally, this study yielded yet another significant discovery.

The flow region in impingement jets is typically split into three areas: the free jet region, the stagnant region, and the wall jet region. The flow develops as wall jets toward the environment and slows down in the flow direction when it exits the stagnation zone.

The thickness of the boundary layer is progressively growing in the meantime. In other words, the fixed jet impingement can only successfully cool the region it reaches because the Nu number dramatically drops from the standstill to the wall. The wall jet effect, however, becomes more pronounced in this area as the separation between the array centers and the two stopping locations diminishes. Examining the average Nu value on the line drawn at X/L=0.25m in this Figure 4.21 makes it obvious.

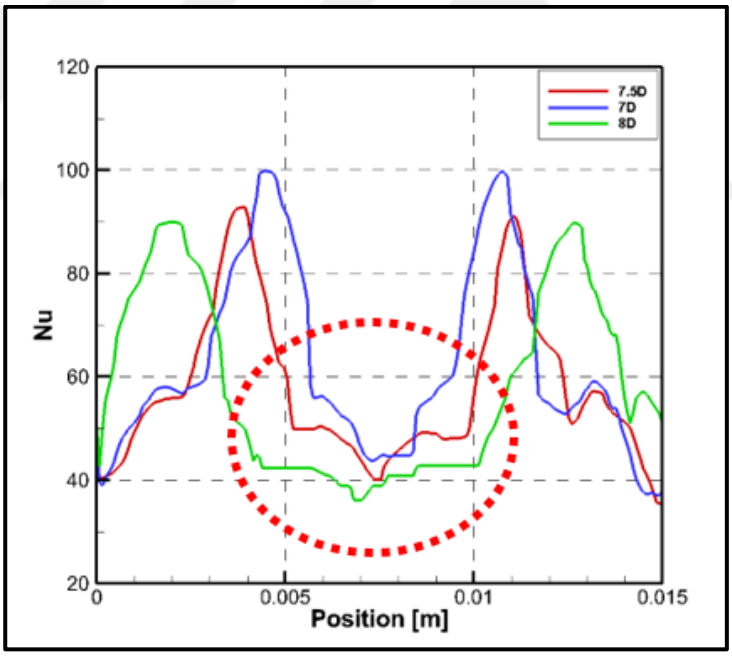

Figure 4.21 The Time-averaged Nu Distribution at X/L=0.25

When the Re 4000 Figure 4.21 is closely inspected, it is clear that as the center distance decreases, a narrower region experiences the rapid fall following the greatest Nu number at the standstill point. (It is shown with a red dashed line) Additionally, it can be observed that the jet wall effect - the lowest Nu value from this region - increases as the space

between the centers gets smaller. This holds true for the other two realized Re values as well. Additionally, it was found that as the Re number increased, the average Nu values that formed increased.

Table 4-1 Table of results for all analyses

Impact Ang.	Re Num.	Distance (D)	Avg. Nu Num.	Avg. Pres. Drop Num.
30°	3000	7.5	24.5	0.13
30°	4000	7.5	26.2	0.22
30°	5000	7.5	31.2	0.36
30°	7000	7.5	38.7	0.87
30°	10000	7.5	48.8	1.69
45°	4000	7.5	27.5	0.33
45°	7000	7.5	40.1	0.99
45°	10000	7.5	50.2	1.88
60°	4000	7.5	28.8	0.35
60°	7000	7.5	42.6	1.26
60°	10000	7.5	**53.1**	**2.21**
30°	4000	7	26.8	0.25
30°	7000	7	39.6	0.91
30°	10000	7	49.9	1.72
30°	4000	8	**19.7**	**0.19**
30°	7000	8	35.2	0.84
30°	10000	8	44.4	1.65

Table 4-1 compiles the findings of all conducted studies. According to the findings, 30° impact angles, 8D oscillator distance, and Re number had the lowest values while 60° impact angles and 10000 Re numbers had the highest values for pressure drop and heat transmission. The outcomes also demonstrate that a 30° impact angle between the oscillators in the model reduces the distance between them, improving both heat transfer and pressure differential.

CHAPTER 5

CONCLUSION&DISCUSSION

Fluidic oscillators are devices that use fluid use fluid flow to generate oscillations and have numerous applications in fields such as air conditioning, aircraft control, and flow control systems. They are a type of fluidic amplifier that can amplify small input signals to produce a larger output, making them useful in situations where it is desirable to control the flow of a fluid without the use of mechanical components. These devices are relatively simple and inexpensive to construct and can operate over a wide range of frequencies and temperatures. Different types of fluidic oscillators exist, each with its own unique characteristics and suitability for different applications.

The aim of this study was to investigate the heat transfer performance and fluid dynamics of a microchannel heat exchanger using two fluidic oscillators to improve heat transfer performance in impinging jet cooling. The study varied the angle of the fluidic oscillator with the channel and the distance between the two oscillators. The study used water as the working fluid, with an inlet temperature of 300 K and a constant heat flux of $q' = 10^6$ W/m^2 applied to the impingement surface, which had an area of 9D×15D. In this study, the angle of the fluidic oscillator with the channel (30°, 45°, 60°) and the distance between the two oscillators (7D, 7.5D, 8D) were varied and examined.

The CFD analysis results of a classical fluidic oscillator geometry indicate that oscillating the jet flow in the jet impingement cooling process enhances the heat transfer performance. Increasing the impact angle results in increased pressure drop and turbulence, leading to an increase in the time-averaged Nu value. Additionally, reducing the distance between the arrays positively affected heat transfer.

The study compared the results of the design change with the reference model, yielding the following observations:

- A 11.85% increase in Nu was observed for Re 4000 when the impact angle was 60°, compared to the reference study. When compared for Re 10000, this improvement was observed to be 12.5% for an impact angle of 60°.

- For a reduced distance (7D) between the oscillator outlet centers compared to the reference model, an improvement of 5.77% was observed in heat transfer for Re 4000.

- A decrease in the average Nu value by 26.9% was observed compared to the reference study when the distance between the oscillator outlet centers increased (8D).

In this study, the conditions that produced the best performance were fixed oscillator spacing of 7.5D and a 60° impact angle. Additionally, the best performance is seen when the impact angle (30) is set and the oscillators are spaced 7D apart. Because the analyses were time-dependent and took too long, not all combinations were examined within the parameters of this study. Because of the analysis's enormous calculation domain and dense solution mesh, parametric analysis is not appropriate. Future research, however, will yield significant results by analyzing the possible smallest distance between oscillator centers and the greatest impact angle.

Overall, the research indicates that fluid oscillators may be a useful tool for enhancing the efficiency of heat transfer in microchannel heat exchangers. The findings show how crucial it is to choose the fluid oscillator geometry including the impact angle and spacing between the oscillators carefully in order to get the best heat transfer efficiency.

Future uses for fluid oscillators have the potential to make them a significant technological advancement. Energy harvesting is one promising area in which liquid oscillators can transform the kinetic energy of moving liquids into electrical energy. This can be especially helpful in locations with a constant flow of fluid, such pipelines or streams. Fluid oscillators can also be utilized in environmental monitoring to identify and gauge fluid flow rates. Liquid oscillators may be used to produce the necessary vibrations or

oscillations in medical equipment like respirators and blood pressure monitors. Fluid oscillators can be used in aviation to regulate airflow through aerodynamic surfaces, enhancing the effectiveness of aircraft or other aviation vehicles. Additionally, it is considered to be a crucial tool for semiconductor industry problem-solving as technology advances. Overall, the adaptability and prospective applications of liquid oscillators suggest that this technology will continue to be significant in a range of future sectors and applications.

In the context of this study, it is crucial to assess potential advancements in heat exchangers. Future heat exchanger performance can be significantly enhanced by the use of fluid oscillators. Improved heat transfer efficiency can result from these devices' periodic fluid motion, which can increase heat transfer rates and lower thermal resistance.

Enhancing fluid mixing is one potential use for fluid oscillators in heat exchangers. By creating chaotic mixing patterns, fluid oscillators can increase the surface area in contact with the hot and cold fluids, aiding in more efficient heat transmission. This can be especially helpful in situations where the fluids have extremely different characteristics or temperatures, like in air conditioning or refrigeration systems.

Fluid oscillators may also be used in heat exchangers to lessen the buildup of deposits and fouling on the heat transfer surfaces. Fluid oscillations can prevent boundary layers and stagnant zones from forming, which can encourage the accumulation of deposits and fouling. Fluid oscillators can prevent or limit the formation of these deposits by promoting flow and mixing, which improves heat transfer performance over time. The flow of the S-ducts, which are employed in aviation, is shown to not enter the heat exchanger uniformly, particularly in the header sections that connect the Heat-Exchanger. The employment of fluid oscillators in such circumstances can aid in obtaining a more homogenous distribution at the input. With all of this in mind, it is clear how crucial the location of fluid oscillators will be in the future. As a result, the testing infrastructure to be used in this area and the outcomes of numerical studies are crucial.

REFERENCES

[1] Dewan, A. & Srivastava, P., "A review of heat transfer enhancement through flow disruption in a microchannel," Journal of Thermal Science, *vol. 24*, no. 3, pp. 203–214, 2015.

[2] Camci, C. & Herr, F., "Forced convection heat transfer enhancement using a self-oscillating impinging planar jet," J Heat Transfer, *vol. 124*, no. 4, pp. 770–782, 2002.

[3] Bergles, A. E. & Mem, H., "995 Max Jakob Memorial Award Lecture Heat Transfer Enhancement-The Encouragement and Accommodation of High Heat Fluxes," ASME, *vol 119*, no. 1, 1997.

[4] Hossain, M. A., Prenter, R., Lundgreen, R. K., Ameri, A., Gregory, J. W., & Bons, J. P., "Experimental and numerical investigation of sweeping jet film cooling," J Turbomach, *vol. 140*, no. 3, 2018.

[5] Lienhard, J.H., "Liquid jet impingement," Ann. Rev. Heat Transfer, *vol. 6*, pp. 199-270. 1995.

[6] Shukla, A. K., & Dewan, A., "Flow and thermal characteristics of jet impingement: Comprehensive review," International Journal of Heat and Technology, *vol. 35*, no. 1, pp. 153–166, Mar. 2017.

[7] Dogruoz, B. M. Experimental and Numerical Investigation of Turbulent Heat Transfer due to Rectangular Impinging Jets Item Type text, Doctoral dissertation. The University of Arizona. 2005

[8] Wu, Y., Yu, S., & Zuo, L., "Large eddy simulation analysis of the heat transfer enhancement using self-oscillating fluidic oscillators," Int J Heat Mass Transfer, *vol. 131*, pp. 463–471, 2019.

[9] Andino, M. Y., Lin, J. C., Washburn, A. E., Whalen, E. A., Graff, E. C., & Wygnanski, I. J., "Flow separation control on a full-scale vertical tail model using sweeping jet actuators," in 53rd AIAA Aerospace Sciences Meeting, 2015.

[10] Ostermann, F., Woszidlo, R., Nayeri C. N., & Paschereit, C. O., "Experimental comparison between the flow field of two common fluidic oscillator designs," in 53rd AIAA Aerospace Sciences Meeting, 2015.

[11] Gregory, J. W., & Tomac, M. N., "A review of fluidic oscillator development and application for flow control," in 43rd Fluid Dynamics Conference, 2013.

[12] Ghanami, S., & Farhadi, M., "Fluidic Oscillators' Applications, Structures and Mechanisms-A review Multiphase flow simulation with LBM View project Capability of fluidic oscillators to enhance heat transfer View project Fluidic Oscillators' Applications, Structures and Mechanisms-A review," Nano Micro Scales, *vol. 7*, no. 1, pp. 9–27, 2019.

[13] Tomac, N.M. Internal Fluid Dynamics and Frequency Characteristics of Feedback-Free Fluidic Oscillators. Doctoral dissertation. The Ohio State University. 2013

[14] Bellhouse, B. J., "A High Efficiency Membrane Oxygenator And Pulsatile Pumping System, And Its Application To Animal Trials," American Society for Artificial Internal Organs, *vol. 19*, no. 1, pp. 72–79, 1973.

[15] Gardon, R., & Cobonpue, J., "Impingement Cooling From a Circular Jet in a Cross Flow," Proceedings of 2nd International Heat Transfer Conference, pp. 719–730, 1962.

[16] Gardon, R., and Akfırat, J.C., “The Role of Turbulence in Determining the Heat Transfer Characteristics of Impinging Jets,” Int J Heat Mass Transf, *vol. 8*, pp. 1261–1272, 1965.

[17] Sieber, M., Ostermann, F., Woszidlo, R., Oberleithner, K., & Paschereit, C. O., “Lagrangian Coherent Structure in the Flow Field of a Fluidic Oscillator,” Phys. Rev. Fluids, *vol. 1*, 1979.

[18] Hossain, M. A., Prenter, R., Lundgreen, R. K., Ameri, A., Gregory, J. W., & Bons, J. P., “Experimental and numerical investigation of sweeping jet film cooling,” J Turbomach, *vol. 140*, no. 3, Mar. 2018.

[19] Seo, J. H., & Mittal, R., “Computational modeling and analysis of sweeping jet fluidic oscillators,” in 47th AIAA Fluid Dynamics Conference, 2017.

[20] Hossain M. A., Prenter, R., Lundgreen, R. K., Ameri, A., Gregory, J. W., & Bons, J. P.,“Effects of roughness on the performance of fluidic oscillators,” in AIAA SciTech Forum - 55th AIAA Aerospace Sciences Meeting, 2017.

[21] Tomac, M. N., & Gregory, J. W., “Internal jet interactions in a fluidic oscillator at low flow rate,” Exp Fluids, *vol. 55*, no. 5, 2014.

[22] Uzol, O. & Camci, C., “Experimental and computational visualization and frequency measurements of the jet oscillation inside a fluidic oscillator,” J Visualization, *vol. 5*, 2002.

[23] Bobusch, B. C., Woszidlo, R., Krüger, O., & Paschereit, C. O., “Numerical investigations on geometric parameters affecting the oscillation properties of a fluidic oscillator,” in 21st AIAA Computational Fluid Dynamics Conference, 2013.

[24] Woszidlo, R., Nawroth, H., Raghu S., & Wygnanski, I. J., "Parametric Study of Sweeping Jet Actuators for Separation Control," 5th Flow Control Conference, 2010.

[25] Metka, M., & Gregory, J. W., "Drag reduction on the 25-deg Ahmed model using fluidic oscillators," Journal of Fluids Engineering, Transactions of the ASME, *vol. 137*, no. 5, May 2015.

[26] Choephel, T., Coder, J., & Maughmer, M. D., "Airfoil Boundary-Layer Flow Control Using Fluidic Oscillators," in 30th AIAA Applied Aerodynamics Conference, pp. 44–54, 2012.

[27] Lin J. C., "Full-scale testing of active flow control applied to a vertical tail," in Journal of Aircraft, *vol. 56*, no. 4, pp. 1376–1386, 2019.

[28] Phillips, E., Woszidlo, R., & Wygnanski, I., "The Dynamics of Separation Control on a Rapidly Actuated Flap," 5th Flow Control Conference, 2010.

[29] Cerretelli, C., Gharaibah, E., Toplack, G., Gupta, A., & Wuerz, W., "Unsteady Separation Control for Wind Turbine Applications at Full Scale Reynolds Numbers," 47th AIAA Aerospace Exposition, 2009.

[30] Raman, G., Packiarajan, S., Papadopoulos, G., Weissman, C., & Raghu, S., "Jet thrust vectoring using a miniature," The Aeronautical Journal, pp. 129–138, 2005.

[31] Mcmanus, K. R., Poinsoti, T., & Candeli, S. M., "A review of active control of combustion instabilities," Progress in Energy and Combustion Science, *vol. 19*, pp. 1-29, 1993.

[32] Guyot, D., Bobusch, B., Paschereit, C. O., & Raghu, S., "Active Combustion Control Using a Fluidic Oscillator for Asymmetric Fuel Flow Modulation," 44th AIAA Joıint Propulsion Conference,2008.

[33] Park, T., Kara, K., & Kim, D., "Flow structure and heat transfer of a sweeping jet impinging on a flat wall," Int J Heat Mass Transf, *vol. 124*, pp. 920–928, 2018.

[34] Hossain, M. A., Agricola, L. M., Ameri, A., Gregory, J. W., & Bons, J. P., "Effects of curvature on the performance of sweeping jet impingement heat transfer," in AIAA Aerospace Sciences Meeting, 2018.

[35] Mohammadshahi, S., Samsam, H., Cai, T., & Kim, K. C., "Experimental and numerical study on flow characteristics and heat transfer of an oscillating jet in a channel," Int J Heat Fluid Flow, *vol. 86*, 2020.

[36] Ghanami, S., & Farhadi, M., "Heat transfer enhancement in a single-pipe heat exchanger with fluidic oscillators," J Therm Anal Calorim, *vol. 140*, no. 3, pp. 1107–1119, 2020.

[37] Lundgreen, R. K., Hossain, M. A., Prenter, R., Bons, J. P., J. Gregory, & Ameri, A., "Impingement heat transfer characteristics of a sweeping jet," in AIAA SciTech Forum - 55th AIAA Aerospace Sciences Meeting, 2017.

[38] Iachachene, F., Mataoui, A., & Halouane, Y., "Numerical investigations on heat transfer of self-sustained oscillation of a turbulent jet flow inside a cavity," J Heat Transfer, *vol. 137*, no. 10, 2015.

[39] O'Donovan, T. S., & Murray, D. B., "Fluctuating fluid flow and heat transfer of an obliquely impinging air jet," Int J Heat Mass Transfer, *vol. 51*, no. 25–26, pp. 6169–6179, 2008.

[40] Fatoyinbo, H. O., "Microfluidic devices for cell manipulation," Microfluidic Devices for Biomedical Applications, pp. 283–350, 2013.

CURRICULUM VITAE

PERSONAL INFORMATION

Name Surname : Furkan YEŞİL
Date of Birth :
Phone :
E-mail :

EDUCATION

Bachelor : Eskişehir Osmangazi University / ESKİŞEHİR
Master Degree : Ankara Yıldırım Beyazıt University

TOPICS OF INTEREST

- Computational Fluid Dynamics
- Computational Heat Transfer

PUBLICATIONS

- **Furkan Yeşil,** Veli Çelik, "In Microchannel Heat Exchanger Performance Enhancement with Fluidic Oscillator Investigation by Transient Regime" III. International Liberty Inderdisciplinary Studies Conference, 13-15 January 2023, Miami.


ANKARA YILDIRIM BEYAZIT ÜNİVERSİTESİ
1992